Article

Cancer Cell

# $O_2^{\bullet -}$ and $H_2O_2$-Mediated Disruption of Fe Metabolism Causes the Differential Susceptibility of NSCLC and GBM Cancer Cells to Pharmacological Ascorbate

## Graphical Abstract

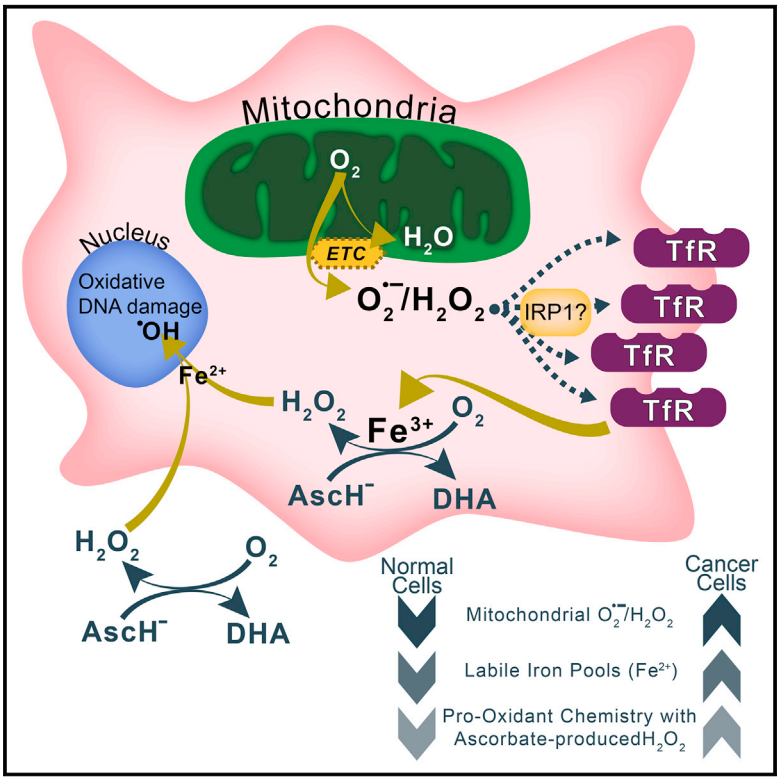


## Highlights

- High-dose ascorbate sensitizes NSCLC and GBM cells to radio-chemotherapy
- $O_2^{\bullet -}$ and $H_2O_2$ increase labile iron causing cancer cell-selective ascorbate toxicity
- Therapeutic levels of ascorbate are achievable and well tolerated in GBM and NSCLC
- Cancer cell oxidative metabolism can be targeted with ascorbate for cancer therapy

## Authors

Joshua D. Schoenfeld, Zita A. Sibenaller, Kranti A. Mapuskar, ..., John M. Buatti, Douglas R. Spitz, Bryan G. Allen

## Correspondence

douglas-spitz@uiowa.edu (D.R.S.), bryan-allen@uiowa.edu (B.G.A.)

## In Brief

Schoenfeld et al. show that cancer cells are selectively sensitive to ascorbate due to their altered redox-active iron metabolism. They present preclinical and clinical data demonstrating the feasibility, tolerability, and potential efficacy of pharmacological ascorbate for treating glioblastoma and non-small cell lung cancer.

Schoenfeld et al., 2017, Cancer Cell *31*, 1–14
April 10, 2017 
http://dx.doi.org/10.1016/j.ccell.2017.02.018

CellPress

Please cite this article in press as: Schoenfeld et al., $O_2^{\bullet-}$ and $H_2O_2$-Mediated Disruption of Fe Metabolism Causes the Differential Susceptibility of NSCLC and GBM Cancer Cells to Pharmacological Ascorbate, Cancer Cell (2017), http://dx.doi.org/10.1016/j.ccell.2017.02.018

Cancer Cell
Article



# $O_2^{\bullet-}$ and $H_2O_2$-Mediated Disruption of Fe Metabolism Causes the Differential Susceptibility of NSCLC and GBM Cancer Cells to Pharmacological Ascorbate

Joshua D. Schoenfeld,[1] Zita A. Sibenaller,[1] Kranti A. Mapuskar,[1] Brett A. Wagner,[1] Kimberly L. Cramer-Morales,[1] Muhammad Furqan,[2] Sonia Sandhu,[2] Thomas L. Carlisle,[2] Mark C. Smith,[1] Taher Abu Hejleh,[2] Daniel J. Berg,[2] Jun Zhang,[2] John Keech,[3] Kalpaj R. Parekh,[3] Sudershan Bhatia,[1] Varun Monga,[2] Kellie L. Bodeker,[1] Logan Ahmann,[1] Sandy Vollstedt,[1] Heather Brown,[1] Erin P. Shanahan Kauffman,[2] Mary E. Schall,[2] Ray J. Hohl,[2] Gerald H. Clamon,[2] Jeremy D. Greenlee,[4] Matthew A. Howard,[4] Michael K. Shultz,[5] Brian J. Smith,[6] Dennis P. Riley,[7] Frederick E. Domann,[1] Joseph J. Cullen,[3] Garry R. Buettner,[1] John M. Buatti,[1] Douglas R. Spitz,[1,8,*] and Bryan G. Allen[1,*]

[1]Free Radical and Radiation Biology Program, Department of Radiation Oncology
[2]Division of Hematology, Oncology, and Blood & Marrow Transplantation, Department of Internal Medicine
[3]Department of Surgery
[4]Department of Neurosurgery
[5]Department of Radiology
[6]Departmet of Biostatistics
Holden Comprehensive Cancer Center, The University of Iowa, Iowa City, IA 52242, USA
[7]Galera Therapeutics, Malvern, PA 19355, USA
[8]Lead Contact
*Correspondence: douglas-spitz@uiowa.edu (D.R.S.), bryan-allen@uiowa.edu (B.G.A.)
http://dx.doi.org/10.1016/j.ccell.2017.02.018

## SUMMARY

Pharmacological ascorbate has been proposed as a potential anti-cancer agent when combined with radiation and chemotherapy. The anti-cancer effects of ascorbate are hypothesized to involve the autoxidation of ascorbate leading to increased steady-state levels of $H_2O_2$; however, the mechanism(s) for cancer cell-selective toxicity remain unknown. The current study shows that alterations in cancer cell mitochondrial oxidative metabolism resulting in increased levels of $O_2^{\bullet-}$ and $H_2O_2$ are capable of disrupting intracellular iron metabolism, thereby selectively sensitizing non-small-cell lung cancer (NSCLC) and glioblastoma (GBM) cells to ascorbate through pro-oxidant chemistry involving redox-active labile iron and $H_2O_2$. In addition, preclinical studies and clinical trials demonstrate the feasibility, selective toxicity, tolerability, and potential efficacy of pharmacological ascorbate in GBM and NSCLC therapy.

## INTRODUCTION

Intravenous pharmacological doses of ascorbate have recently re-emerged as a potential anti-cancer therapy with clinical trials in ovarian and pancreatic cancer subjects demonstrating tolerability with similar or reduced toxicities, relative to chemotherapy alone (Ma et al., 2014; Monti et al., 2012; Welsh et al., 2013). Preclinical studies with ascorbate have consistently demonstrated cancer cell-selective cytotoxicity in a variety of disease sites (Du et al., 2010; Ma et al., 2014; Riordan et al., 1995). Although the mechanism(s) of selective toxicity remain unknown, mounting evidence suggests that ascorbate toxicity is dependent on the action of ascorbate as a pro-drug for hydrogen peroxide ($H_2O_2$) generation (Chen et al., 2005, 2007; Olney et al., 2013).

### Significance

Despite advances in treatment strategies, 5-year overall survival in NSCLC and GBM has not significantly increased over the last 20 years. Here, we demonstrate that pharmacological ascorbate represents an easily implementable and non-toxic agent that may increase treatment efficacy when combined with standard-of-care radio-chemotherapy in NSCLC and GBM. Furthermore, the mechanism by which ascorbate is selectively toxic to cancer cells versus normal cells is shown to involve alterations in redox-active iron metabolism mediated by mitochondrial $O_2^{\bullet-}$ and $H_2O_2$. As fundamental defects in oxidative metabolism leading to increased steady-state levels of $O_2^{\bullet-}$ and $H_2O_2$ emerge as targetable hallmarks of cancer cells, the current findings support a generalized mechanism for the application of pharmacological ascorbate in cancer therapy.

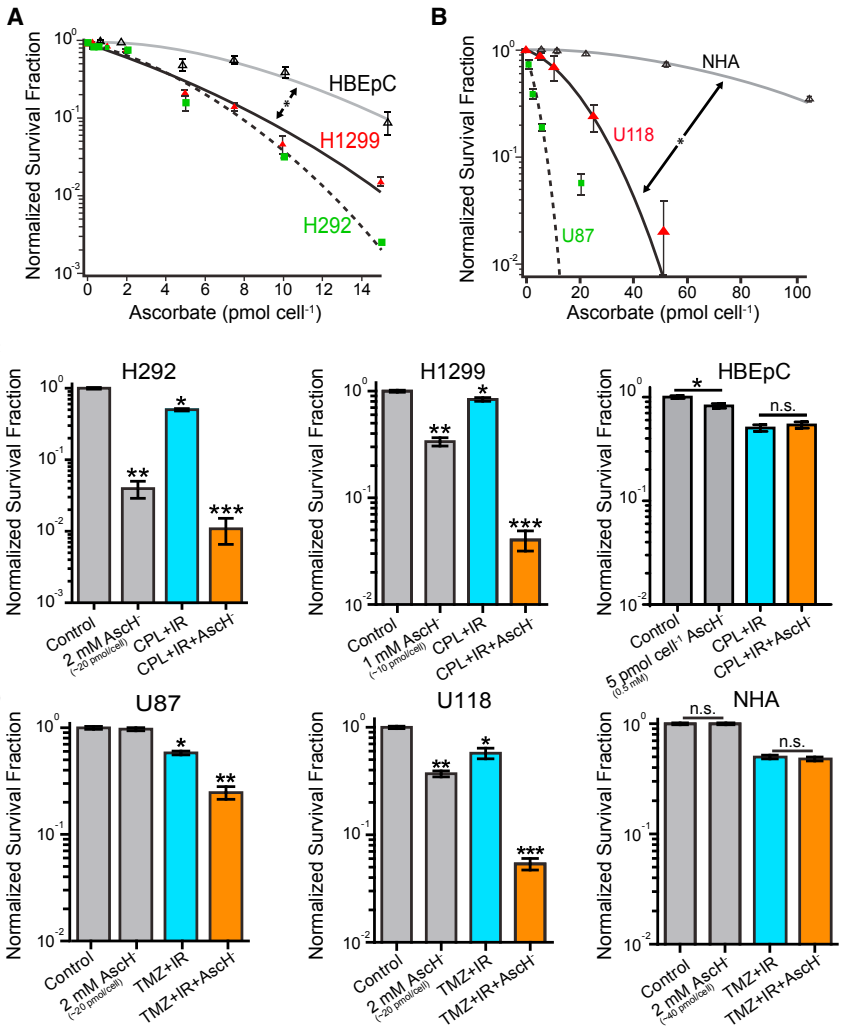


**Figure 1. Ascorbate Selectively Sensitizes NSCLC and GBM Cells, Compared with Normal Cells, to Chemo-Radiation In Vitro**

(A and B) Clonogenic survival post exposure of NSCLC cell lines H1299 and H292 and HBEpCs (A) or GBM cell lines U87 and U118 and NHAs (B) to increasing doses of pharmacological ascorbate for 1 hr.

(C and D) Clonogenic survival of NSCLC and HBEpCs post serial exposure to 5 μM carboplatin for 1 hr, ascorbate for 1 hr, and 2 Gy IR (C). Clonogenic survival of GBM and NHAs post serial exposure to 5 μM temozolomide for 1 hr, ascorbate for 1 hr, and 2 Gy IR (D). For all in vitro studies, n ≥ 3 biological replicates with n = 6 technical replicates per sample.

Data are represented as mean ± SEM. *, **, or *** represent significant differences between untreated control cells and any group denoted with a different symbol, at least $p < 0.05$. n.s., not significant ($p > 0.05$). See also Figure S1.

## RESULTS

### Pharmacological Ascorbate Selectively Sensitizes NSCLC and GBM Cells, Compared to Normal Cells, to Radio-Chemotherapy

The efficacy of ascorbate in preclinical NSCLC and GBM models was assessed using clonogenic survival assays and murine xenografts. Comparisons of the effects of ascorbate in cancer versus normal cells in vitro were performed in identical media preparations due to the dependence of ascorbate toxicity on medium constituents including pyruvate, metal ions, pH, and serum (Olney et al., 2013; Buettner, 1988; Nath et al., 1995; Clément et al., 2001; Mojić et al., 2014). In addition, ascorbate was dosed per cell (pmol cell$^{-1}$), rather than by concentration, due to the dependence of ascorbate and $H_2O_2$ toxicity on cell density (Figure S1A) (Doskey et al., 2015; Spitz et al., 1987). In all in vitro experiments, both dosing metrics are indicated, where available, as concentration-based metrics will be vital in future clinical applications of ascorbate. Importantly, doses utilized to demonstrate mechanistic aspects of ascorbate toxicity all fall within the range of tissue concentrations likely achieved in vivo after intravenous (i.v.) administration (Chen et al., 2008; Kuiper et al., 2014; Campbell et al., 2016).

Exposure of NSCLC cells (H292 and H1299) and GBM cells (U87 and U118) to increasing doses of ascorbate demonstrated dose-dependent clonogenic cell killing (Figures 1A and 1B). In all cases, ascorbate was significantly more toxic to NSCLC and GBM cells, relative to normal human bronchial epithelial primary cells (HBEpCs) or normal human astrocytes (NHAs) (Figures 1A, 1B, and S1B–S1D). Furthermore, ascorbate selectively sensitized NSCLC and GBM cells, but not HBEpC or NHA, to ionizing radiation (IR) combined with chemotherapy (Figures 1C and 1D).

Interestingly, both $H_2O_2$ toxicity and ascorbate oxidation forming $H_2O_2$ are dependent upon metal ion redox chemistry (Buettner and Jurkiewicz, 1996; Du et al., 2015a; Halliwell and Gutteridge, 1990). Furthermore, there is increasing evidence that perturbations in cancer cell oxidative metabolism result in increased steady-state levels of reactive oxygen species (ROS), including superoxide ($O_2^{\bullet-}$) and $H_2O_2$ (Bize et al., 1980; Szatrowski and Nathan, 1991; Spitz et al., 2000; Aykin-Burns et al., 2009), and that these species may be capable of disrupting cellular iron metabolism leading to increased labile iron pool (LIP) levels (Caltagirone et al., 2001; Ibrahim et al., 2013; Pantopoulos et al., 1997). Indeed, many cancer cells exhibit disruptions in iron metabolism with upregulation of several iron-uptake pathways, such as transferrin receptor (TfR), as well as downregulation of iron export and storage pathways (Torti and Torti, 2013).

The current study examines the role of $O_2^{\bullet-}$- and $H_2O_2$-mediated disruptions in cancer cell iron metabolism in the selective toxicity of pharmacological ascorbate. In addition, this study investigates the safety, tolerability, and potential efficacy of pharmacological ascorbate in combination with standard-of-care radio-chemotherapies in glioblastoma (GBM) and advanced-stage non-small-cell lung cancer (NSCLC) subjects.

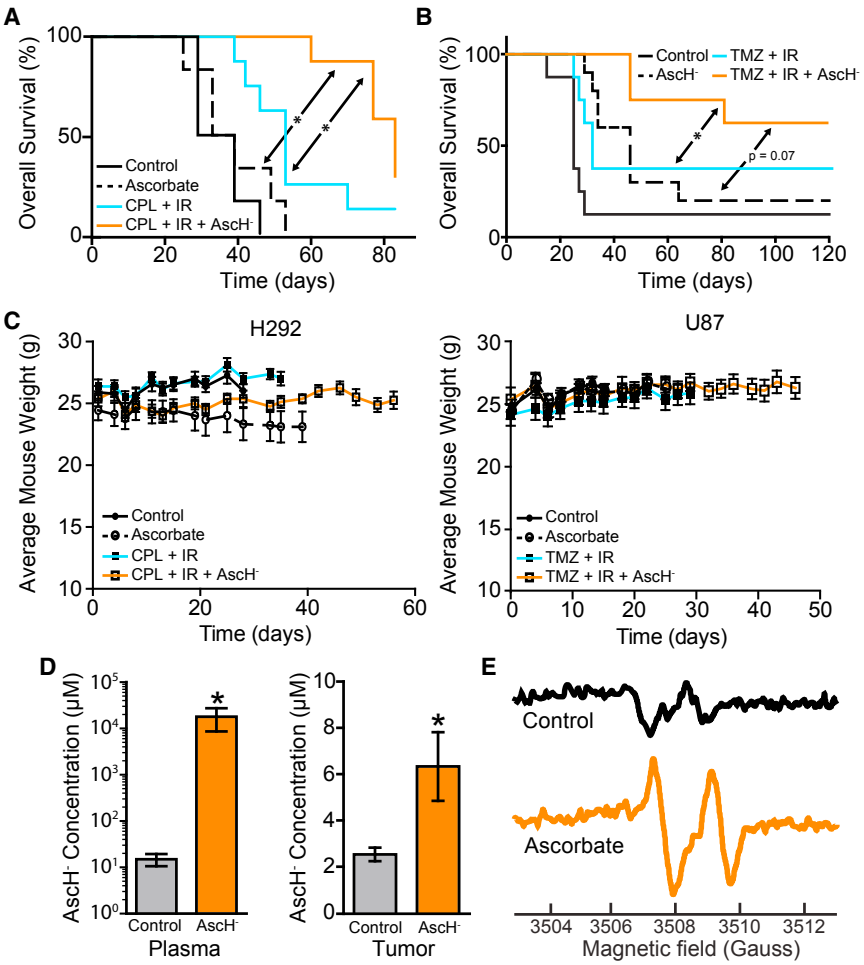


**Figure 2. Ascorbate is Safe and Efficacious in Combination with Radio-Chemotherapy for the Treatment of NSCLC and GBM Cells In Vivo**

(A) Overall survival of mice with H292 xenografts treated with chemo-radiation (5 mg/kg carboplatin weekly, 12 Gy IR/2 fx) with or without ascorbate (4 g/kg ascorbate i.p. or an equivalent osmotic dose of NaCl daily).

(B) Overall survival of mice with U87 xenografts treated with radio-chemotherapy (25 mg/kg temozolomide weekly, 12 Gy IR/2 fx) with or without ascorbate (4 g/kg i.p. ascorbate or an equivalent osmotic dose of NaCl daily). For (A) and (B), mice were killed when tumors reached 15 mm in the greatest diameter.

(C) Average weight of mice with H292 or U87 xenografts.

(D) Plasma and tumor ascorbate concentrations from mice with H292 xenografts collected at a single time point 1 hr after i.p. ascorbate treatment (4 g/kg or an equivalent osmotic dose of NaCl).

(E) Representative result of electron paramagnetic resonance spectra monitoring for the ascorbyl radical at $g$ = 2.0 from the cerebrospinal fluid from healthy nude athymic female mice at a single time point 1 hr after i.p. treatment with ascorbate (4 g/kg) or an equivalent dose of NaCl. For all in vivo studies, mice n $\geq$ 7 per treatment group. For all ex vivo studies, n $\geq$ 3 mice per group with n $\geq$ 3 technical replicates per sample.

Data are represented as mean ± SEM. * represents significant difference, at least $p < 0.05$.

NSCLC and GBM xenograft studies demonstrated that ascorbate (4 g/kg intraperitoneal [i.p.] injection, daily) combined with radio-chemotherapy significantly increased overall survival compared with radio-chemotherapy alone (Figures 2A and 2B). Ascorbate treatment was well tolerated as monitored by mouse weight (Figure 2C), and i.p. delivery significantly increased ascorbate levels in the plasma, tumor, and cerebrospinal fluid in samples collected at a single time point 1 hr (therefore, not necessarily peak levels) after ascorbate administration (Figures 2D and 2E). These data establish the tolerability and efficacy of pharmacological ascorbate in preclinical models of NSCLC and GBM and support the existence of an intrinsic mechanism of selective ascorbate toxicity in cancer versus normal cells.

## Selective Ascorbate Toxicity is Not Dependent on Dehydroascorbate Uptake

A recent report by Yun et al. (2015) suggested that the differential uptake of the two-electron oxidation product of ascorbate, dehydroascorbic acid (DHA), by glucose transporters (GLUTs) in *KRAS* and *BRAF* mutant isogenic colorectal cells mediates the energetic crisis underlying the differential toxicity of ascorbate in cancer versus normal cells (Yun et al., 2015). However, in the more complex genetic background used in the current report (Table S1), *KRAS* status alone did not predict ascorbate sensitivity in NSCLC cells (Figure S1B). Furthermore, competitive inhibition of GLUT transporters with 20 mM 2-deoxy-D-glucose (2-DG) did not suppress ascorbate toxicity and appeared to potentially enhance ascorbate toxicity, suggesting that uptake through GLUTs does not contribute to the observed effects in these model systems (Figure 3A). Importantly, previous reports demonstrate inhibition of DHA uptake by 20 mM 2-DG (Rumsey et al., 1997) and, in the current model, 20 mM 2-DG inhibited total ascorbate/DHA uptake by 37% (Figure 3B). Furthermore, DHA was significantly less toxic compared with ascorbate (Figure 3C). Taken together, these results support the conclusion that ascorbate, not DHA, is the cancer cell-selective toxic species in the current model system.

## Ascorbate Toxicity is Dependent on the Intracellular Reactions of $H_2O_2$ and Redox-Active Labile Iron

Confirming the generality of the previously reported dependence of ascorbate toxicity on the generation of $H_2O_2$ (Chen et al., 2005, 2007; Olney et al., 2013), ascorbate toxicity in NSCLC and GBM cells was inhibited by exogenous catalase or adenoviral-mediated overexpression of catalase or glutathione peroxidase 1 (Figures 4A–4C and S2A). As both $H_2O_2$ toxicity and ascorbate oxidation to generate $H_2O_2$ are dependent upon metal ion redox chemistry (Buettner and Jurkiewicz, 1996; Du et al., 2015a; Halliwell and Gutteridge, 1990), it follows that ascorbate toxicity may be dependent on intracellular pro-oxidant metal ion

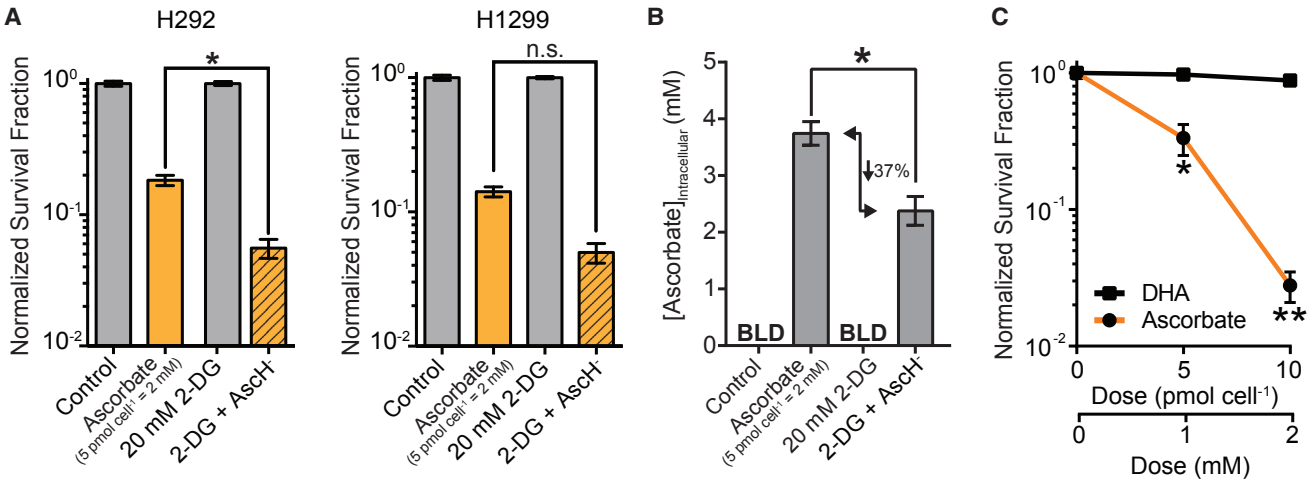


**Figure 3. GLUT-Mediated DHA Uptake Does Not Mediate Ascorbate Toxicity**

(A and B) DHA uptake via glucose transporters (GLUTs) was competitively inhibited with 20 mM 2-deoxy-D-glucose (2-DG) for 15 min prior and during exposure to 5 pmol cell$^{-1}$ (2 mM) ascorbate for 1 hr and then measured for clonogenic survival in H292 and H1299 NSCLC cell lines (A) or measured for total intracellular ascorbate ($AscH^-$, $AscH^{\bullet -}$, and DHA) in H1299 cells (B) by a kinetic spectrophotometric assay (BLD, below the limit of detection).

(C) Clonogenic survival of H1299 cells exposed to equivalent increasing doses (per cell and concentration) of $AscH^-$ or DHA for 1 hr. For all clonogenic survival assays, n ≥ 3 biological replicates with n = 6 technical replicates per sample. For $AscH^-$/DHA uptake, n ≥ 3 with n = 3 technical replicates per sample. Data are represented as mean ± SEM. * represents significant difference, at least $p < 0.05$. n.s., not significant ($p > 0.05$). See also Table S2.

chemistry, as has previously been suggested in breast and prostate cancer (Verrax and Calderon, 2009). Indeed, chelators that inhibit redox cycling of iron (desferrioxamine, DFO; diethylenetriamine-pentaacetic acid, DTPA) (Buettner, 1986) significantly inhibited ascorbate toxicity in both NSCLC and GBM cell lines (Figures 4D, S2B, and S2C).

To further test the role of redox-active metal ions, H292 cells were pre-incubated for 3 hr with DFO/DTPA or EDTA, known to enhance iron redox cycling (Buettner, 1986), and washed prior to ascorbate treatment or chelator treated medium was added to the cells only during ascorbate exposure, providing conditions under which the chelators were either primarily intracellular or extracellular during ascorbate exposure. Intracellular DFO/DTPA inhibited ascorbate toxicity, while intracellular EDTA enhanced ascorbate toxicity relative to control or extracellular chelators (Figures 4E and S3). In addition, increasing the LIP with exogenous $Fe^{2+}$, as ferrous ammonium sulfate (FAS), sensitized H292 NSCLC cells to ascorbate (Figure 4F). These results support the hypothesis that the combination of $H_2O_2$ and intracellular redox-active metal ions is necessary and sufficient for ascorbate toxicity and suggest that differences in cellular iron metabolism regulating the level of redox-active iron may mediate the mechanism of cancer cell-selective ascorbate toxicity.

## Disturbances in Oxidative Metabolism Selectively Sensitize Cancer Cells to Ascorbate through Disruptions in Iron Metabolism

There is a growing body of literature demonstrating that disruptions in cancer cell oxidative metabolism results in increased steady-state levels of ROS, including $O_2^{\bullet -}$ and $H_2O_2$ (Bize et al., 1980; Springer, 1980; Spitz et al., 2000; Aykin-Burns et al., 2009; Szatrowski and Nathan, 1991). Furthermore, $O_2^{\bullet -}$ and $H_2O_2$ have been proposed, under certain conditions, to disrupt homeostatic cellular iron metabolism (Caltagirone et al., 2001; Ibrahim et al., 2013; Pantopoulos et al., 1997), and a growing body of literature suggests that, in general, cancer cells demonstrate increased levels of intracellular labile iron (Torti and Torti, 2013). Given these previous observations, we hypothesized that increased mitochondrial-derived ROS leading to disruptions in cellular iron metabolism may underlie the selective mechanism of ascorbate toxicity.

Supporting this hypothesis, following lobectomy, fresh frozen NSCLC tissue demonstrated increased steady-state levels of $O_2^{\bullet -}$, as determined by superoxide dismutase (SOD) mimetic (GC4419)-inhibitable dihydroethidium (DHE) oxidation (Figures 5A, S4, and S5A), as well as increased labile iron (Figures 5B and S4) compared with adjacent normal tissue. These results support the hypothesis that increased steady-state levels of $O_2^{\bullet -}$ lead to an increased LIP that could sensitize cancer cells to ascorbate in human tissues.

To directly test this hypothesis, the CRISPR/Cas9 system was utilized to delete the mitochondrial SOD gene, *SOD2*, in A549 NSCLC cells (*SOD2*$^{-/-}$) (Figures S5B and S5C), which are relatively resistant to ascorbate-mediated cell killing. As predicted, *SOD2*$^{-/-}$ cells demonstrated increased steady-state levels of $O_2^{\bullet -}$ (Figure 5C), a significantly increased LIP (Figure 5D), as well as increased susceptibility to pharmacological ascorbate-induced clonogenic cell killing (Figure 5E). Demonstrating the generality of this finding, identical results were obtained in HEL 92.1.7 erythroleukemia *SOD2*$^{-/-}$ cells (Figures S5D–S5I). The above results demonstrate that increased steady-state levels of $O_2^{\bullet -}$ are capable of disrupting cellular iron metabolism, increasing the intracellular LIP, and sensitizing ascorbate-resistant cancer cell lines.

Consistent with results from a large immunohistochemical study demonstrating increased TfR levels in NSCLC tissue compared with adjacent normal lung tissue (Kukulj et al., 2010), NSCLC and GBM cell lines demonstrated increased TfR

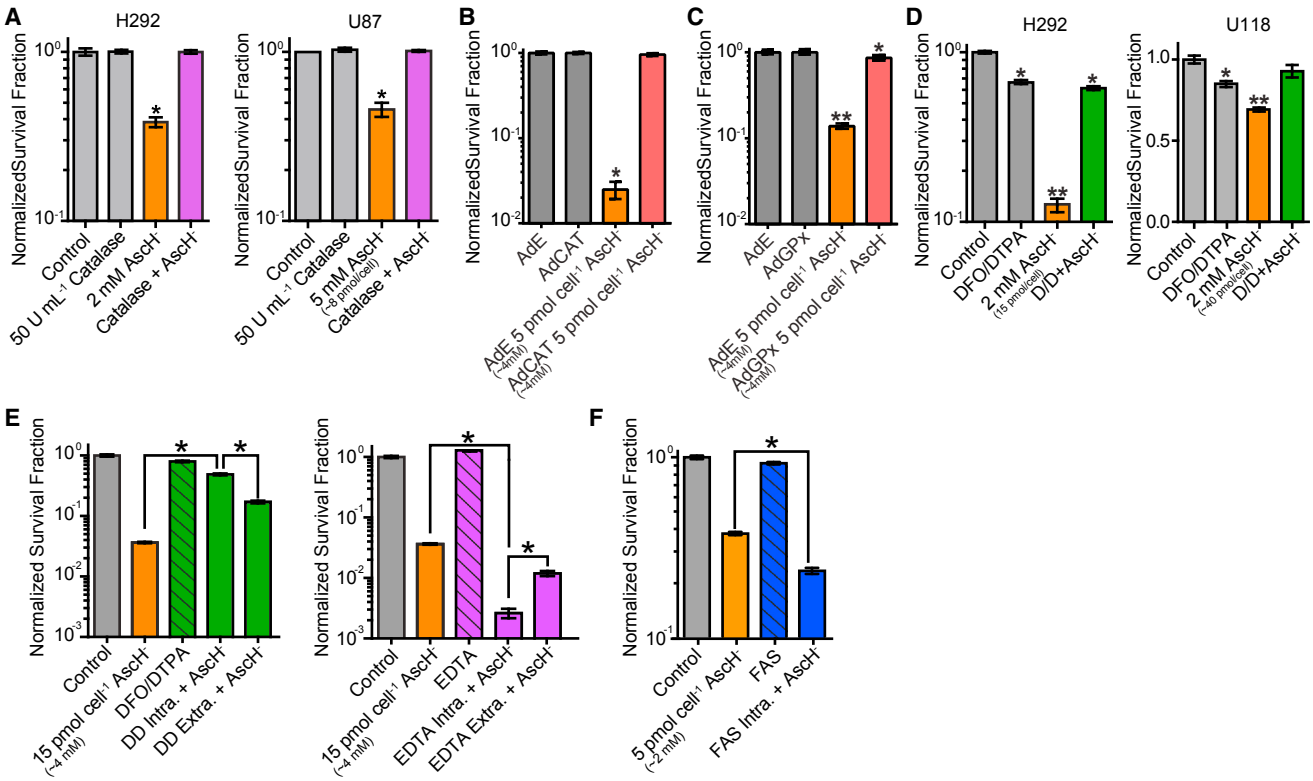


**Figure 4. The Combination of $H_2O_2$ and Redox-Active Labile Iron Is Necessary and Sufficient for Ascorbate Toxicity**

(A) Clonogenic survival of H292 or U87 cells following co-exposure to 50 U/mL bovine catalase ± ascorbate for 1 hr.

(B and C) Clonogenic survival of H1299 cells transiently overexpressing (25 MOI adenoviral-mediated [Ad] transduction) catalase (B) or GPx1 (C) following exposure to ascorbate for 1 hr. For GPx1 experiments, 30 nM sodium selenite was added to the basal medium in all groups after transduction and during clonogenic growth.

(D) Clonogenic survival of H292 and U118 cells treated with 200 μM DFO and 1 mM DTPA for 3 hr followed by 1 hr exposure to ascorbate in the continued presence of the chelators.

(E and F) H292 cells were exposed to 200 μM DFO/1 mM DTPA, 1 mM EDTA (E), or 250 μM FAS (F) for 3 hr and washed prior to ascorbate exposure (intracellular) or medium was pretreated for 3 hr in the absence of cells and co-exposed to cells only during 1 hr ascorbate exposure (extracellular) and then plated for clonogenic survival. For all in vitro studies, n ≥ 3 biological replicates with n = 6 technical replicates per sample.

Data are represented as mean ± SEM. * represents significant difference, at least $p < 0.05$. See also Figures S2 and S3.

levels compared with HBEpCs or NHAs, respectively (Figure 5F and S5J). Interestingly, in cancer cells, increased TfR is seen in the context of increased labile iron content (Figure 5B). Further supporting the role of increased $O_2^{\bullet-}$ in disruption of iron metabolism in cancer cells, *SOD2*$^{-/-}$ cells exhibited increased TfR protein levels compared with WT parental cells in the context of an increased basal LIP (Figures 5D, 5G, S5G, and S5H). Demonstrating the causal role of cancer cell-specific TfR upregulation in ascorbate sensitivity, siRNA knock down of TfR significantly decreased the cellular LIP and protected H1299 cells from ascorbate toxicity (Figures 5H and 5I).

To overcome technical limitations of genetic approaches in non-immortalized human cells, a pharmacological approach was utilized to increase mitochondrial $O_2^{\bullet-}$ in NHAs by inhibiting electron flow through complex III of the electron transport chain (ETC) with antimycin A (AntA). Exposure of NHAs to 25 μM AntA significantly increased DHE oxidation, cellular labile iron, and sensitized NHAs to ascorbate-mediated cell killing (Figure 5J). Consistent with the proposed mechanism that the lower LIP in normal cells limits ascorbate toxicity, exposure of NHAs to exogenous $Fe^{2+}$, as FAS, increased the intracellular LIP and sensitized NHAs to ascorbate toxicity (Figure 5K). Together, these data support the conclusion that cancer cell-specific increases in LIP, as a result of perturbed mitochondrial $O_2^{\bullet-}$ metabolism, significantly contributes to the differential sensitivity of human lung and brain cancer cells to ascorbate toxicity.

## Ascorbate Selectively Increases Cancer Cell LIP through $H_2O_2$-Mediated Disruptions of Fe-S-Containing Proteins

In addition to basal differences in labile iron (Figure 5B), NSCLC and GBM cells demonstrated significant dose-dependent ascorbate-induced increases in cellular LIP that were not seen in HBEpCs or NHAs (Figures 6A, 6B, and S6A). This finding was consistent with previous ex vivo studies showing that ascorbate increased labile iron in pancreatic cancer xenograft lysates (Boyer and McCleary, 1987; Moser et al., 2014). Importantly, although these doses induce cancer cell clonogenic cell killing, metabolic viability determined with trypan blue dye or the reduction of resazurin 1–1.5 hr post ascorbate exposure was

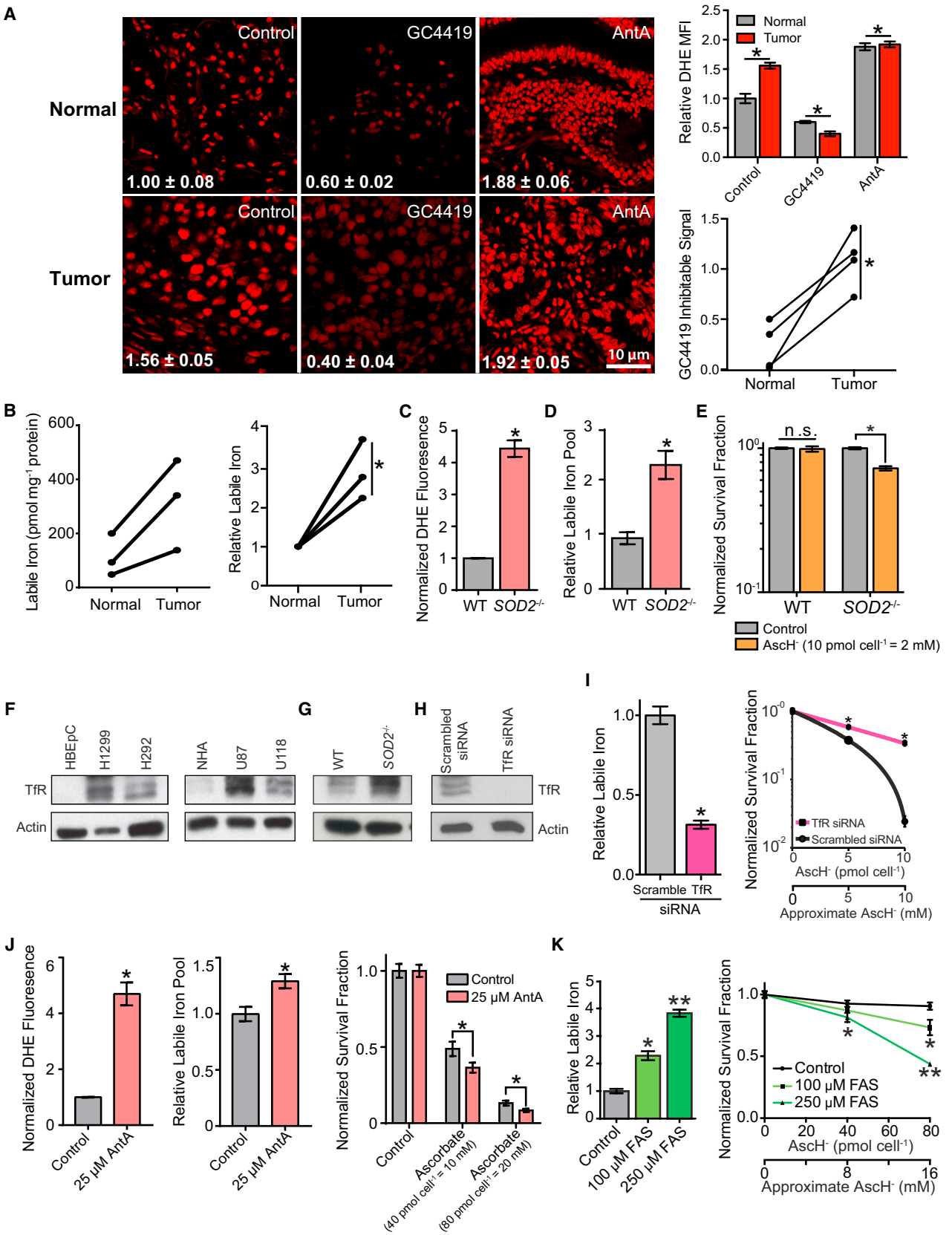


(legend on next page)

unchanged, demonstrating that changes in LIP seen at 1 hr are not a consequence of metabolic cell death (Figure S6B). In intact cells, disruption of the integrity of Fe-S cluster proteins may contribute to ascorbate-mediated increases in LIP as shown by the inactivation of the Fe-S cluster-containing proteins aconitase and mitochondrial ETC complexes I and II, while having no effect on ETC complex IV activity, which contains no Fe-S clusters (Figures 6C and 6D). The loss of Fe-S cluster protein activity as well as the increased LIP seen in ascorbate-treated cancer cells was prevented by catalase overexpression (Figures 6C, 6E, and 6F) but not SOD1 or SOD2 (Figure 6G), implicating $H_2O_2$ as the causative agent in ascorbate-induced increases in LIP.

Consistent with LIP redox cycling contributing to the selective toxicity of ascorbate in cancer cells, ascorbate increased steady-state levels of $H_2O_2$ (as measured by the $H_2O_2$-sensitive fluorescent probe PeroxyOrange-1) from baseline in NSCLC cells while remaining unchanged in HBEpCs, a phenomenon not seen with excess genuine $H_2O_2$ used as a positive control (Figures 6H, S6C, and S6D). In addition, adenoviral-mediated overexpression of Ft heavy chain (Ft-H; contains ferroxidase activity required for iron storage) significantly decreased basal LIP compared with cells overexpressing Ft light chain (Ft-L; lacks ferroxidase activity) or control cells (Figures 6I and 6J). Interestingly, only Ft-H overexpression inhibited ascorbate-induced increases in LIP as well as ascorbate-mediated toxicity (Figures 6K, 6L, and S6E).

## Pharmacological Ascorbate is Safe, Tolerable, and Potentially Efficacious in Combination with Radio-Chemotherapy in GBM and Advanced-Stage NSCLC

These preclinical studies in GBM led to a phase I clinical trial assessing the safety and tolerability of pharmacological ascorbate in combination with IR and temozolomide in GBM subjects (NCT 01752491) (Table S2; Figure S7A). Following maximum safe surgical resection or biopsy (if unresectable), subjects received radiation (daily), temozolomide (daily), and i.v. ascorbate infusions (three times a week) for approximately 7 weeks (radiation phase; Stupp et al., 2005). For each subsequent subject, ascorbate doses were escalated during the radiation phase (15–125 g infusion) with a 20 mM target plasma concentration (infusion dose denoted next to each subject number in Figure 7A; Welsh et al., 2013). Following conclusion of the radiation phase, all subjects were dose escalated to achieve $\geq$ 20 mM plasma ascorbate in combination with temozolomide for approximately 28 weeks (for a total therapy duration of ~35 weeks; Figure 7A). The desired mean therapeutic blood level was achieved in all subjects receiving the 87.5 g infusions (Figures 7B, S7B, and S7C).

Pharmacological ascorbate was safe and well tolerated in all 13 subjects who participated in the trial with minimal grade 3 and 4 toxicities, which compared favorably with Stupp et al. (2005) (Tables S3 and S4). Non-hematological toxicities observed in the phase 1 trial during the radiation phase included grade 2 and 3 fatigue, grade 2 and 3 nausea, grade 2 infection, and grade 3 vomiting. In the adjuvant phase, observed toxicities included grade 2 fatigue, grade 2 nausea, grade 1 vomiting, grade 3 leukopenia, and grade 3 neutropenia. No serious adverse events in the radiation phase or adjuvant phase were ascribed to pharmacological ascorbate treatment and all subjects maintained their performance status throughout the treatment.

Although the small number of subjects prevent a statistically significant assessment of efficacy (11 subjects; 2 subjects were removed from longevity analysis due to limited protocol-dictated therapy due to unrelated co-morbidities), average progression-free survival (PFS) currently stands at 13.3 months (median, 9.4 months) versus the historical median PFS of 7 months (Stupp et al., 2005), and average overall survival is currently 21.5 months (median, 18.2 months) versus the historical median of 14 months. Furthermore, four subjects remain alive, with one showing no evidence of disease based on MRI (Figures 7A and 7C). Importantly, the characteristics of the subject population were not significantly different than the subject characteristics from Stupp et al. (2005) (Table S5).

**Figure 5. Increased Steady-State Levels of Mitochondrial $O_2^{\cdot-}$ Disrupt Cellular Iron Homeostasis Increasing the LIP and Sensitizing Cancer Cells to Ascorbate**

(A) 10 μm sections of NSCLC or adjacent normal tissue were stained with 10 μM DHE on the same slide for 30 min prior to analysis by confocal microscopy. For treatment groups, tissue sections were pretreated for 30 min with 0.5 μM GC4419 SOD mimetic prior to DHE exposure. For a positive control, tissue sections were incubated with 10 μM antimycin A during DHE staining. The mean fluorescence intensity (MFI) of ≥200 nuclei from six randomly selected areas was quantified using ImageJ software.

(B) NSCLC and adjacent normal tissue was assayed for labile iron content by electron paramagnetic resonance quantification of the high spin state $Fe^{3+}$-DFO complex ($g$ = 4.3, 100 K) against a standard curve and normalized to total tissue protein. Each data point represents the average of triplicate technical replicates.

(C and D) Levels of DHE oxidation (C) and baseline cellular LIP (D) of parental and *SOD2*$^{-/-}$ A549 cells quantified by flow cytometry and normalized to the parental cell line.

(E) Clonogenic survival of parental and *SOD2*$^{-/-}$ A549 cells following exposure to 10 pmol cell$^{-1}$ (2 mM) ascorbate for 1 hr.

(F–H) Western blot analysis of TfR protein levels (25 μg total protein) in HBEpC/NSCLC cells and NHA/GBM cells (F), parental and *SOD2*$^{-/-}$ A549 cells (G), and H1299 cells (H) treated with 25 pmol siRNA/dish with actin protein loading controls. For all blots, the images were cropped and extra lanes were removed.

(I) Basal LIP in H1299 cells treated with 25 pmol scrambled or TfR siRNA per dish and clonogenic survival of H1299 cells treated with 25 pmol scrambled or TfR siRNA per dish post 1 hr exposure to ascorbate.

(J) Normalized DHE fluorescence and relative labile iron in NHAs exposed to 25 μM AntA for 30 min prior to flow cytometry analysis and clonogenic survival of NHAs following co-exposure to 25 μM AntA and ascorbate for 30 min.

(K) NHAs exposed to 100 μM or 250 μM FAS for 3 hr prior to LIP quantification by flow cytometry or washed with PBS before exposure to ascorbate for 1 hr in fresh full medium and then plated for clonogenic survival. For all in vitro studies, unless noted above, n ≥ 3 biological replicates with n ≥ 3 technical replicates per sample.

Data are represented as mean ± SEM. *, ** represents significant differences between untreated control cells and any group denoted with a different symbol, at least $p < 0.05$. See also Figures S4 and S5.

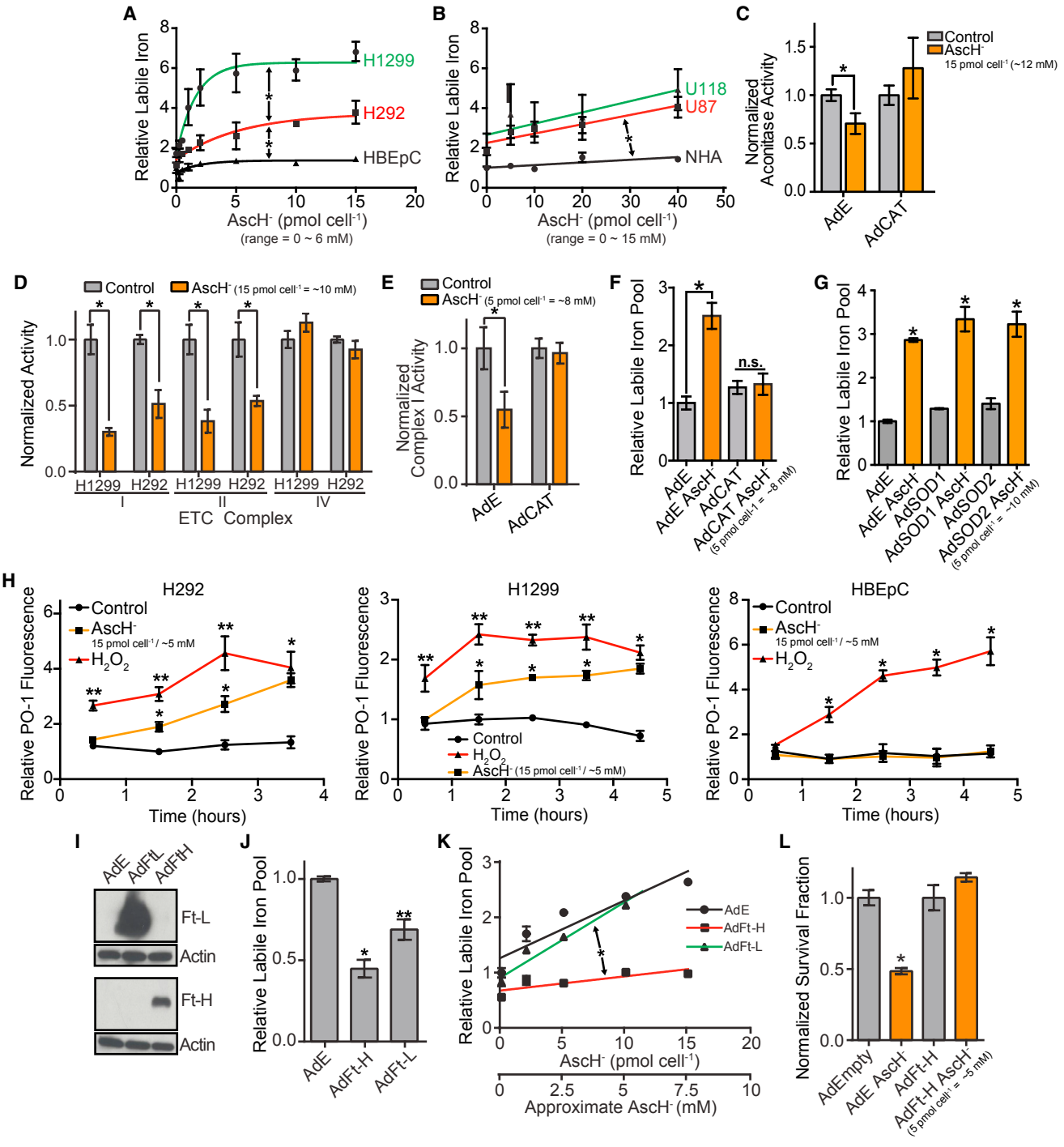


**Figure 6. Ascorbate Selectively Increases Cancer Cell LIP via $H_2O_2$-Mediated Disruptions of Fe-S Clusters and Overexpression of Ft-H Protects Against Ascorbate Toxicity**

(A and B) Relative intracellular LIP levels following exposure to increasing doses of ascorbate in HBEpCs and NSCLC cells (A) or NHAs and GBM cells (B) as assayed by flow cytometry and normalized to HBEpCs or NHAs, respectively.

(C–E) Quantification of total cellular aconitase (C) or ETC complex I, II, and IV activity (D) after exposure to 15 pmol cell$^{-1}$ (~8 mM) ascorbate for 1 hr in NSCLC cell lysates of control cells or cells transiently overexpressing catalase (50 MOI adenoviral-mediated [Ad] transduction 36 hr prior) (C and E).

(F and G) Quantification of the relative cellular LIP of H1299 cells overexpressing (50 MOI Ad transduction 36 hr prior) an empty vector or catalase (F) or SOD1 and SOD2 (G) as assayed by flow cytometry.

(H) Relative oxidation of $H_2O_2$-sensitive fluorescent probe PO-1 in H292, H1299, or HBEpCs treated with 15 pmol cell$^{-1}$ ascorbate (~5 mM) once or 100 μM $H_2O_2$ every 30 min by flow cytometry.

(I) Representative western blot of H1299 cells overexpressing (20 MOI Ad transduction 36 hr prior) empty, Ft-L, or Ft-H with actin protein loading control.

*(legend continued on next page)*

Most interestingly, a companion study published by Stupp et al. (2005) analyzed the methylation status of the $O^6$-methylguanine-DNA methyltransferase gene (*MGMT*) promoter (Hegi et al., 2005), and demonstrated a significant reduction in survival in GBM subjects receiving concurrent radiation and temozolomide that lacked *MGMT* promoter methylation (median overall survival = 12.7 versus 21.7 months). In the Stupp et al. (2005) trial, *MGMT* promoter methylation was absent in 57% of the GBM subjects (Hegi et al., 2005). In comparison, *MGMT* promoter methylation was absent in 73% of the subjects in the current phase I clinical trial and median overall survival for subjects lacking *MGMT* promoter methylation is 23.0 months (versus 12.7 months in Hegi et al., 2005). In addition, three of eight subjects lacking *MGMT* promoter methylation in the current trial remain alive, with one showing no evidence of disease based on MRI (Figures 7A and 7D).

Furthermore, the initial results (n = 14 subjects) from a phase II clinical trial assessing the efficacy of pharmacological ascorbate with platinum-doublet chemotherapy in advanced-stage NSCLC (NCT 02420314) (Figure S8A; Table S6) also demonstrate promising results in achieving therapeutic ascorbate blood levels (16.4 ± 0.5 mM; Figures S8B and S8C) and achieved a disease control rate of 93% and a confirmed objective response rate of 29%, compared with historical controls with 40% disease control rates and 15%–19% confirmed objective response rates (Figures 7E and 7F) (Schiller et al., 2002; Sandler et al., 2006).

## DISCUSSION

The combination of high-dose i.v. and oral ascorbate was first proposed as a potential anti-cancer agent in 1976 (Cameron and Pauling, 1976). However, two randomized clinical trials testing the efficacy of high-dose oral ascorbate failed to demonstrate any effect on survival (Creagan et al., 1979; Moertel et al., 1985). Subsequent pharmacokinetic studies demonstrated the inability of oral ascorbate dosing to reach therapeutic plasma levels (Padayatty et al., 2004). This finding revitalized interest in ascorbate as an adjuvant to cancer therapy and demonstrated the need to confirm plasma levels of ascorbate to ensure therapeutic concentrations are achieved (Welsh et al., 2013). With this more complete understanding of ascorbate pharmacokinetics, this work, and others on pancreatic and ovarian cancer, have consistently demonstrated selective toxicity to cancer cells compared with normal cells both in vitro and in vivo (Du et al., 2010; Monti et al., 2012; Welsh et al., 2013; Ma et al., 2014). Furthermore, the results of the current clinical trials, together with the results of all previous clinical trials that we are aware of, continue to demonstrate a lack of ascorbate toxicity in normal tissue when combined with chemotherapy or radio-chemotherapies. In addition, preliminary data from both the GBM and NSCLC trials presented here show promising results for potentially increasing efficacy of current treatment regimens.

The mechanism underlying the cancer cell-selective toxicity of ascorbate has remained incompletely understood since Cameron and Rotman (1972) first hypothesized the usefulness of pharmacological ascorbate in cancer therapy. Recently, Yun et al. (2015) hypothesized that the selective toxicity of ascorbate in *KRAS* and *BRAF* mutant clones was facilitated by increased GLUT-mediated uptake of dehydroascorbate and subsequent $NAD^+$ depletion and energetic crisis. In the current study, GLUT-mediated DHA uptake demonstrated a minimal role in ascorbate toxicity in these model systems. Furthermore, consistent with the mechanism of ROS-mediated disruptions in cellular iron metabolism underlying the selective toxicity of ascorbate, *KRAS* and *BRAF* mutant cells have been suggested to demonstrate increased mitochondrial-derived ROS (Corazao-Rozas et al., 2013; Liou et al., 2016).

The results of the current study demonstrate that increased LIP levels, resulting from increased mitochondrial $O_2^{\bullet-}$ and $H_2O_2$, significantly contribute to the cancer cell-selective toxicity of pharmacological ascorbate combined with standard radiochemotherapy in NSCLC and GBM models. The theoretical model (Figure 8) illustrates that increased labile iron in cancer cells results in increased oxidation of ascorbate to generate $H_2O_2$ capable of further exacerbating the differences in labile iron in cancer versus normal cells. This occurs, at least partially, due to $H_2O_2$-mediated disruption of Fe-S cluster-containing proteins. The increased levels of $H_2O_2$, in the presence of an increased LIP, result in increased Fenton chemistry to generate hydroxyl radicals ($^{\bullet}OH$) causing oxidative damage. These reactions most likely occur at sites of macromolecule-associated weakly chelated redox-active iron due to the diffusion-limited kinetics of $^{\bullet}OH$.

In normal cells, with reduced levels of basal and ascorbate-mediated increases in $O_2^{\bullet-}$, $H_2O_2$, and labile iron, $H_2O_2$ is rapidly metabolized prior to participating in pro-oxidant chemistry. Under normal cell conditions, therefore, the pro-oxidant actions of ascorbate are neutralized by increased $H_2O_2$ metabolism (Doskey et al., 2016) in the presence of a restricted LIP, and the anti-oxidant actions of ascorbate prevail. In support of this, pharmacological ascorbate has been proposed to protect IR-mediated damage to jejunal crypts in mice (Du et al., 2015b) and decrease chemotherapy-associated adverse events in ovarian cancer subjects (Ma et al., 2014).

Since cancer cells, in general, have been hypothesized to demonstrate increased steady-state levels of $O_2^{\bullet-}$ and $H_2O_2$ due to fundamental defects in oxidative metabolism (Bize et al., 1980; Spitz et al., 2000; Aykin-Burns et al., 2009; Oberley et al., 1980) and increased labile iron (Torti and Torti, 2013;

(J and K) Baseline LIP (J) and LIP after 1 hr ascorbate exposure (K) in H1299 cells overexpressing (20 MOI Ad transduction 36 hr prior) empty, Ft-L, or Ft-H as assayed by flow cytometry.

(L) Clonogenic survival of H1299 cells overexpressing (20 MOI Ad transduction 36 hr prior) empty or Ft-H exposed to 5 pmol $cell^{-1}$ (~2–3 mM) for 1 hr. For all in vitro studies, $n \geq 3$ biological replicates with $n \geq 3$ technical replicates per sample. Western blots are representative images of at least three replicates. For both blots, images were cropped to remove non-specific bands and to limit image size.

Data are represented as mean ± SEM. *,** represent significant differences between untreated control cells and any group denoted with a different symbol, at least $p < 0.05$. See also Figures S6.

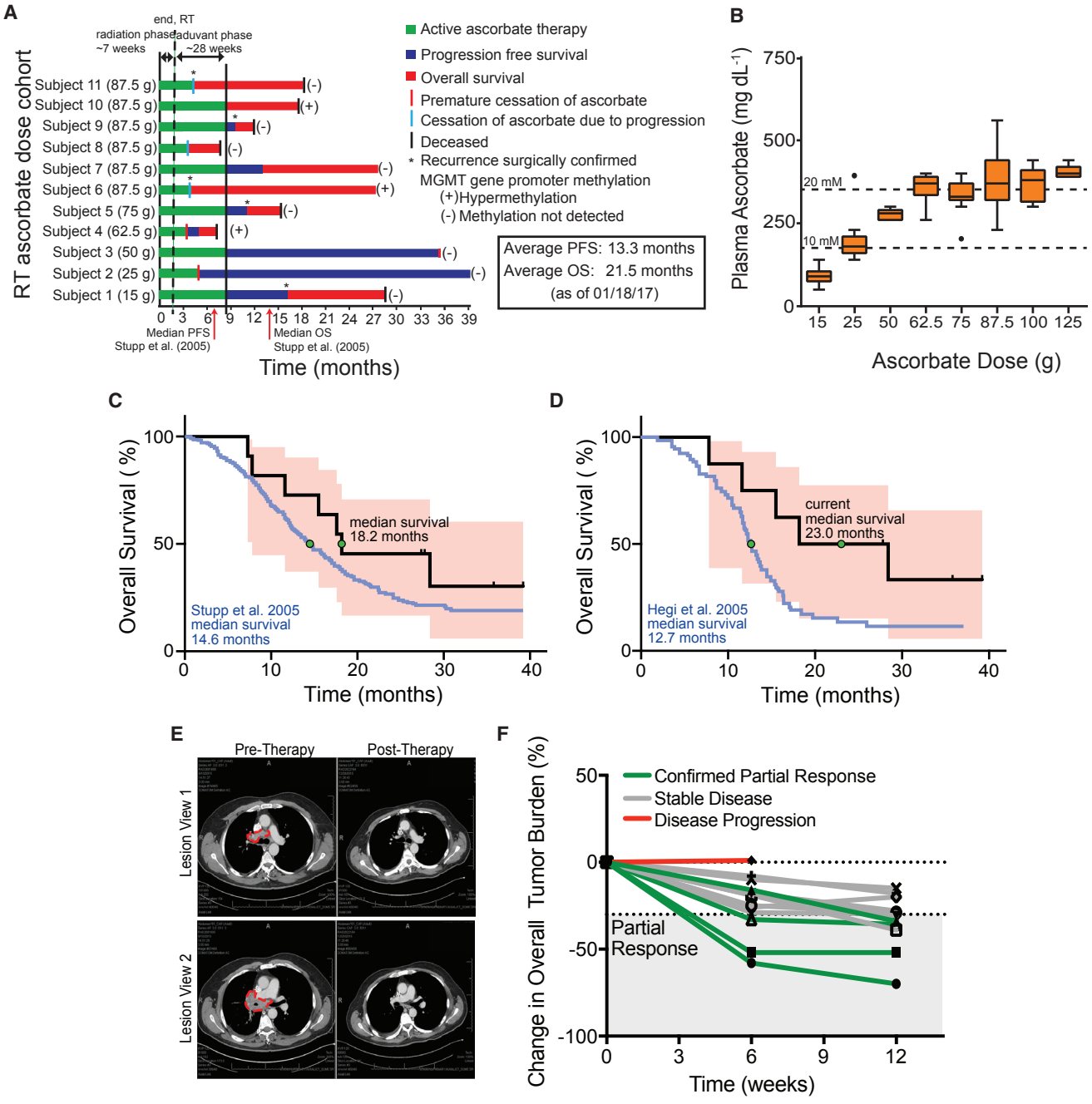


**Figure 7. Pharmacological Ascorbate Is Safe and Well Tolerated when Combined with Standard Therapy in the Treatment of GBM and NSCLC**

(A) Progression-free survival (PFS) and overall survival (OS) of GBM subjects treated with pharmacological ascorbate, radiation, and temozolomide. Subjects were treated with temozolomide daily with concurrent radiation therapy (radiation phase) for ~7 weeks followed by ~28 additional weeks of temozolomide therapy (adjuvant phases), for a total of ~35 weeks. The doses denoted adjacent to each subject number indicates the ascorbate dose received during the radiation phase dose-escalation study. All subjects' doses were increased to achieve target plasma levels ≥ 20 mM during the adjuvant phase. Historical median PFS is 7 months and OS is 14.6 months. The green bars indicate the duration of active ascorbate therapy, blue bars indicate PFS, and red bars indicate OS. The vertical red lines indicate pre-mature cessation of the clinical trial due to personal reasons; vertical light blue lines indicate cessation of the trial due to progression of disease while receiving ascorbate therapy; vertical black lines indicate death; * indicates surgical confirmation of recurrence; (+) indicates *MGMT* gene promoter hypermethylation; and (–) indicates absence of *MGMT* gene promoter methylation.

(B) GBM subjects' plasma ascorbate levels were measured from blood samples collected directly following ascorbate infusion during dose escalation and throughout ascorbate therapy. Boxplots are calculated using the Tukey method. The line and box represent the median value ± the 25th and 75th percentiles or the interquartile range (IQR). Whiskers represent 1.5 times IQR. Any data points outside 1.5 times IQR are represented by individual dots.

(C) Survival curve for 11 GBM subjects (black line) with 95% confidence intervals (red shading) compared with Stupp et al. (2005) historical controls (blue line).

*(legend continued on next page)*

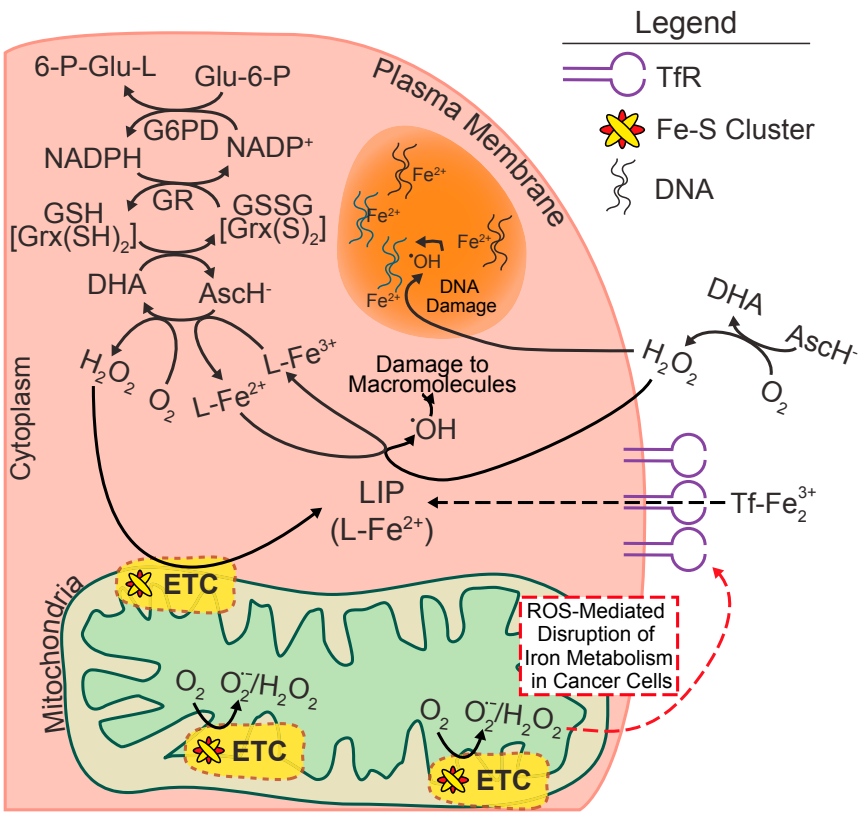


**Figure 8. Proposed Mechanism of Pharmacological Ascorbate Cancer-Cell-Selective Toxicity**

Dashed lines represent multi-step processes not illustrated in the model. In brief, cancer cells demonstrate increased levels of redox-active labile iron due to increased steady-state levels of mitochondrial $O_2^{\bullet-}$ and $H_2O_2$, which are capable of disrupting cellular iron homeostasis. Oxidation of ascorbate produces $H_2O_2$ that reacts with the increased LIP in cancer cells to mediate Fenton chemistry and cause oxidative damage to cellular macromolecules (i.e., DNA, protein, lipids). Due to the diffusion-limited kinetics of $HO^{\bullet}$ species, redox-active iron chelated by these macromolecules most likely represent the most prevalent site of damage. Furthermore, $H_2O_2$ produced from ascorbate oxidation selectively increases the cancer cell LIP, partially by disrupting Fe-S clusters, further exacerbating the differences in LIP available for oxidation reactions and mediate ascorbate toxicity in cancer versus normal cells. In this model, endogenous ascorbate recycling mechanisms are driven by reducing equivalents from nicotinamide adenine dinucleotide phosphate (NADPH) and glutathione (GSH) and/or glutaredoxin (Grx) allowing for the continuous production of $H_2O_2$. Glu, glucose; G6PD, glucose-6-phosphate dehydrogenase; GR, glutathione reductase; L-Fe, weakly chelated redox-active iron; Tf, Transferrin.

Caltagirone et al., 2001; Ibrahim et al., 2013; Pantopoulos et al., 1997), the current findings, combined with similar findings in pancreas and ovarian cancer (Monti et al., 2012; Welsh et al., 2013; Ma et al., 2014), continue to support the potential for the general application of pharmacological ascorbate in cancer therapy. Given these data, ascorbate may represent an easily implementable addition to current anti-cancer therapies, and further large-scale clinical studies are warranted to determine the overall efficacy of ascorbate in NSCLC and GBM. Finally, manipulations of redox-active metal ions in cancer cells may represent both a target and a biomarker for predicting responses to pharmacological ascorbate in cancer therapy.

## STAR★METHODS

Detailed methods are provided in the online version of this paper and include the following:

- KEY RESOURCES TABLE
- CONTACT FOR REAGENT AND RESOURCE SHARING
- EXPERIMENTAL MODEL AND SUBJECT DETAILS
  - Cell Lines and Primary Cultures
  - In Vivo Mouse Studies
  - Clinical Trials
- METHOD DETAILS
  - Ascorbate and Ascorbate Exposure
  - Ionizing Radiation
  - Clonogenic Survival, Viability, and Metabolic Activity Assays
  - Murine Xenograft Models
  - Ascorbate Quantification
  - CSF Ascorbate Radical Electron Paramagnetic Resonance (EPR)
  - Adenovirus Transduction
  - Radiolabeled $^{14}$C-EDTA Uptake
  - Human Tissue Sample Collection and Inclusion Metrics
  - Tissue DHE Staining and Quantification
  - Tissue Iron Quantification
  - CRISPR/Cas9-Mediated Deletion of SOD2
  - SOD Activity Assay
  - Cellular Labile Iron Pool Quantification
  - Western Blots
  - Transferrin Receptor siRNA
  - Aconitase Activity
  - ETC Complex Activity

(D) Survival curve for 8 GBM subjects whose tumors lacked *MGMT* promoter methylation (black line) with 95% confidence intervals (red shading) compared with Hegi et al. (2005) historical controls (blue line).

(E) Pre- and post-therapy CT images from NSCLC subject 1 illustrating the tumor volume (red dashed line).

(F) Spider plot illustrating therapy responses from the first 14 advanced-stage NSCLC subjects. As per RECIST1.1, partial response is ≥30% reduction in target tumor burden that is maintained for at least 4 weeks. See also Figures S7 and S8, Tables S2–S6.

## SUPPLEMENTAL INFORMATION

Supplemental Information includes eight figures and six tables and can be found with this article online at http://dx.doi.org/10.1016/j.ccell.2017.02.018.

## AUTHOR CONTRIBUTIONS

Conceptualization, J.D.S., D.R.S., and B.G.A.; Methodology, J.D.S., T.A.H., M.F., J.J.C., G.R.B., J.M.B., M.K.S., F.E.D., D.R.S., and B.G.A.; Validation, J.D.S., D.R.S., and B.G.A.; Formal Analysis, J.D.S., G.R.B., and B.J.S.; Investigation, J.D.S., Z.A.S., K.L.C.-M., K.A.M., B.A.W., B.G.A., J.M.B., S.S., T.L.C., M.C.S., T.A.H., M.F., J.Z., J.K., K.R.P., S.B., S.V., H.B., E.P.S.K., M.E.S., R.J.H., G.H.C., J.D.G., M.A.H., and V.M.; Resources, D.P.R.; Data Curation, K.L.B., L.A., and D.J.B.; Writing – Original Version, J.D.S. and D.R.S.; Writing – Review & Editing, J.D.S., D.R.S., and B.G.A.; Visualizations, J.D.S.; Supervision, D.R.S. and B.G.A.; Funding Acquisition, J.J.C., G.R.B., J.M.B., D.R.S., and B.G.A.

## ACKNOWLEDGMENTS

The authors thank Rita Sigmund, Joseph Galbraith, Dr. Michael Knudson, and Dr. Robert Robinson from The University of Iowa (UI) Tissue Procurement Core. The authors also acknowledge Dr. Michael McCormick and Amanda Kalen from the UI Radiation and Free Radical Research Core for performing SOD activity assays and irradiation services, respectively. All flow cytometry data presented herein were obtained at the UI Flow Cytometry Facility, which is a Carver College of Medicine/Holden Comprehensive Cancer Center core research facility at the University of Iowa funded through user fees and the generous financial support of the Carver College of Medicine, Holden Comprehensive Cancer Center, and Iowa City Veteran's Administration Medical Center. We would also like to thank Dr. James Martin for allowing us to utilize his confocal microscope. We would also like to thank Dr. Paul Akhenblit for his help with the resazurin metabolic activity studies. Finally, the authors would like to thank Claire Doskey for thoughtful discussion throughout the studies and Gareth Smith for graphical design assistance. This work is supported by American Society for Radiation Oncology (ASTRO) grant JF2014-1 (to B.G.A.), the Carver Research Program of Excellence in Redox Biology (to D.R.S.), and US NIH grants R01-CA182804 (to D.R.S.), R01-CA184051 (to J.J.C.), R01-CA169046 (to G.R.B.), U01-CA166800 (to J.M.B.), a gift from Ms. Marie Foster/matched by IBM, and CCSG P30-CA086862 to The University of Iowa Holden Comprehensive Cancer Center. J.D.S. was supported by T32-GM007337 (to the University of Iowa Medical Scientist Training Program), and J.D.S. and K.L.C.-M. were supported by T32-CA078586 (to D.R.S.). Dr. Dennis Riley is the Chief Scientific Officer of Galera Therapeutics, which supplied GC4419 SOD mimetic for use in these studies. J.M.B., D.R.S., and B.G.A. have sponsored research agreements with Galera Therapeutics for unrelated projects.

Received: June 3, 2016
Revised: December 13, 2016
Accepted: February 27, 2017
Published: March 30, 2017

## SUPPORTING CITATIONS

The following references appear in the Supplemental Information: Janmaat et al. (2006); Matsubara et al. (2013); Sunaga et al. (2011); Ueda et al. (2008).

## REFERENCES

Ahmad, I.M., Aykin-Burns, N., Sim, J.E., Walsh, S.A., Higashikubo, R., Buettner, G.R., Venkataraman, S., Mackey, M.A., Flanagan, S.W., Oberley, L.W., et al. (2005). Mitochondrial $O_2^{\bullet-}$ and $H_2O_2$ mediate glucose deprivation-induced stress in human cancer cells. J. Biol. Chem. *280*, 4254–4263.

Ahmad, I.M., Abdalla, M.Y., Aykin-Burns, N., Simons, A.L., Oberley, L.W., Domann, F.E., and Spitz, D.R. (2008). 2-Deoxyglucose combined with wild-type p53 overexpression enhances cytotoxicity in human prostate cancer cells via oxidative stress. Free Radic. Biol. Med. *44*, 826–834.

Aykin-Burns, N., Ahmad, I.M., Zhu, Y., Oberley, L.W., and Spitz, D.R. (2009). Increased levels of superoxide and $H_2O_2$ mediate the differential susceptibility of cancer cells versus normal cells to glucose deprivation. Biochem. J. *418*, 29–37.

Birch-Machin, M.A., Briggs, H.L., Saborido, A.A., Bindoff, L.A., and Turnbull, D.M. (1994). An evaluation of the measurement of the activities of complexes I-IV in the respiratory chain of human skeletal muscle mitochondria. Biochem. Med. Metab. Biol. *51*, 35–42.

Bize, I.B., Oberley, L.W., and Morris, H.P. (1980). Superoxide dismutase and superoxide radical in Morris hepatomas. Cancer Res. *40*, 3686–3693.

Boyer, R.F., and McCleary, C.J. (1987). Superoxide ion as a primary reductant in ascorbate-mediated ferritin iron release. Free Radic. Biol. Med. *3*, 389–395.

Buettner, G.R. (1986). Ascorbate autoxidation in the presence of iron and copper chelates. Free Radic. Res. Commun. *1*, 349–353.

Buettner, G.R. (1988). In the absence of catalytic metals ascorbate does not autoxidize at pH 7: ascorbate as a test for catalytic metals. J. Biochem. Biophys. Methods *16*, 27–40.

Buettner, G.R., and Jurkiewicz, B.A. (1996). Catalytic metals, ascorbate and free radicals: combinations to avoid. Radiat. Res. *145*, 532–541.

Caltagirone, A., Weiss, G., and Pantopoulos, K. (2001). Modulation of cellular iron metabolism by hydrogen peroxide: effects of $H_2O_2$ on the expression and function of iron-responsive element-containing mRNAs in B6 fibroblasts. J. Biol. Chem. *276*, 19738–19745.

Cameron, E., and Rotman, D. (1972). Ascorbic acid, cell proliferation, and cancer. Lancet *299*, 542.

Cameron, E., and Pauling, L. (1976). Supplemental ascorbate in the supportive treatment of cancer: prolongation of survival times in terminal human cancer. Proc. Natl. Acad. Sci. USA *73*, 3685–3689.

Campbell, E.J., Vissers, M.C.M., Wohlrab, C., Hicks, K.O., Strother, R.M., Bozonet, S.M., Robinson, B.A., and Dachs, G.U. (2016). Pharmacokinetic and anti-cancer properties of high dose ascorbate in solid tumours of ascorbate-dependent mice. Free Radic. Biol. Med. *99*, 451–462.

Case, A.J., McGill, J.L., Tygrett, L.T., Shirasawa, T., Spitz, D.R., Waldschmidt, T.J., Legge, K.L., and Domann, F.E. (2011). Elevated mitochondrial superoxide disrupts normal T cell development, impairing adaptive immune responses to an influenza challenge. Free Radic. Biol. Med. *50*, 448–458.

Chen, Q., Espey, M.G., Krishna, M.C., Mitchell, J.B., Corpe, C.P., Buettner, G.R., Shacter, E., and Levine, M. (2005). Pharmacologic ascorbic acid concentrations selectively kill cancer cells: action as a pro-drug to deliver hydrogen peroxide to tissues. Proc. Natl. Acad. Sci. USA *102*, 13604–13609.

Chen, Q., Espey, M.G., Sun, A.Y., Lee, J.-H., Krishna, M.C., Shacter, E., Choyke, P.L., Pooput, C., Kirk, K.L., Buettner, G.R., et al. (2007). Ascorbate in pharmacologic concentrations selectively generates ascorbate radical and hydrogen peroxide in extracellular fluid in vivo. Proc. Natl. Acad. Sci. USA *104*, 8749–8754.

Chen, Q., Espey, M.G., Sun, A.Y., Pooput, C., Kirk, K.L., Krishna, M.C., Khosh, D.B., Drisko, J., and Levine, M. (2008). Pharmacologic doses of ascorbate act as a prooxidant and decrease growth of aggressive tumor xenografts in mice. Proc. Natl. Acad. Sci. USA *105*, 11105–11109.

Clément, M.-V., Ramalingam, J., Long, L.H., and Halliwell, B. (2001). The in vitro cytotoxicity of ascorbate depends on the culture medium used to perform the assay and involves hydrogen peroxide. Antioxid. Redox Signal. *3*, 157–163.

Corazao-Rozas, P., Guerreschi, P., Jendoubi, M., André, F., Jonneaux, A., Scalbert, C., Garçon, G., Malet-Martino, M., Balayssac, S., Rocchi, S., et al. (2013). Mitochondrial oxidative stress is the Achilles heel of melanoma cells resistant to Braf-mutant inhibitor. Oncotarget *4*, 1986–1998.

Cramer-Morales, K., Heer, C.D., Mapuskar, K.A., and Domann, F.E. (2015). SOD2 targeted gene editing by CRISPR/Cas9 yields human cells devoid of MnSOD. Free Radic. Biol. Med. *89*, 379–386.

Creagan, E.T., Moertel, C.G., O'Fallon, J.R., Schutt, A.J., O'Connell, M.J., Rubin, J., and Frytak, S. (1979). Failure of high-dose vitamin C (ascorbic acid) therapy to benefit patients with advanced cancer. A controlled trial. N. Engl. J. Med. *301*, 687–690.

Dickinson, B.C., Huynh, C., and Chang, C.J. (2010). A palette of fluorescent probes with varying emission colors for imaging hydrogen peroxide signaling in living cells. J. Am. Chem. Soc. *132*, 5906–5915.

Doskey, C.M., van 't Erve, T.J., Wagner, B.A., and Buettner, G.R. (2015). Moles of a substance per cell is a highly informative dosing metric in cell culture. PLoS One *10*, e0132572.

Doskey, C.M., Buranasudja, V., Wagner, B.A., Wilkes, J.G., Du, J., Cullen, J.J., and Buettner, G.R. (2016). Tumor cells have decreased ability to metabolize $H_2O_2$: implications for pharmacological ascorbate in cancer therapy. Redox Biol. *10*, 274–284.

Du, J., Martin, S.M., Levine, M., Wagner, B.A., Buettner, G.R., Wang, S., Taghiyev, A.F., Du, C., Knudson, C.M., and Cullen, J.J. (2010). Mechanisms of ascorbate-induced cytotoxicity in pancreatic cancer. Clin. Cancer Res. *16*, 509–520.

Du, J., Wagner, B.A., Buettner, G.R., and Cullen, J.J. (2015a). Role of labile iron in the toxicity of pharmacological ascorbate. Free Radic. Biol. Med. *84*, 289–295.

Du, J., Cieslak, J.A., Welsh, J.L., Sibenaller, Z.A., Allen, B.G., Wagner, B.A., Kalen, A.L., Doskey, C.M., Strother, R.K., Button, A.M., et al. (2015b). Pharmacological ascorbate radiosensitizes pancreatic cancer. Cancer Res. *75*, 3314–3326.

Eisenhauer, E.A., Therasse, P., Bogaerts, J., Schwartz, L.H., Sargent, D., Ford, R., Dancey, J., Arbuck, S., Gwyther, S., Mooney, M., et al. (2009). New response evaluation criteria in solid tumours: revised RECIST guideline (version 1.1). Eur. J. Cancer *45*, 228–247.

Epsztejn, S., Kakhlon, O., Glickstein, H., Breuer, W., and Cabantchik, Z.I. (1997). Fluorescence analysis of the labile iron pool of mammalian cells. Anal. Biochem. *248*, 31–40.

Halliwell, B., and Gutteridge, J.M.C. (1990). Role of free radicals and catalytic metal ions in human disease: an overview. Methods Enzymol. *186*, 1–85.

Hegi, M.E., Diserens, A.-C., Gorlia, T., Hamou, M.-F., de Tribolet, N., Weller, M., Kros, J.M., Hainfellner, J.A., Mason, W., Mariani, L., et al. (2005). MGMT gene silencing and benefit from temozolomide in glioblastoma. N. Engl. J. Med. *352*, 997–1003.

Ibrahim, W.H., Habib, H.M., Kamal, H., St Clair, D.K., and Chow, C.K. (2013). Mitochondrial superoxide mediates labile iron level: evidence from Mn-SOD-transgenic mice and heterozygous knockout mice and isolated rat liver mitochondria. Free Radic. Biol. Med. *65C*, 143–149.

Janmaat, M.L., Rodriguez, J.A., Gallegos-Ruiz, M., Kruyt, F.A.E., and Giaccone, G. (2006). Enhanced cytotoxicity induced by gefitinib and specific inhibitors of the Ras or phosphatidyl inositol-3 kinase pathways in non-small cell lung cancer cells. Int. J. Cancer *118*, 209–214.

Kuiper, C., Vissers, M.C.M., and Hicks, K.O. (2014). Pharmacokinetic modeling of ascorbate diffusion through normal and tumor tissue. Free Radic. Biol. Med. *77*, 340–352.

Kukulj, S., Jaganjac, M., Boranic, M., Krizanac, S., Santic, Z., and Poljak-Blazi, M. (2010). Altered iron metabolism, inflammation, transferrin receptors, and ferritin expression in non-small-cell lung cancer. Med. Oncol. *27*, 268–277.

Liou, G.-Y., Döppler, H., DelGiorno, K.E., Zhang, L., Leitges, M., Crawford, H.C., Murphy, M.P., and Storz, P. (2016). Mutant Kras-induced mitochondrial oxidative stress in acinar cells upregulates EGFR signaling to drive formation of pancreatic precancerous lesions. Cell Rep *14*, 2325–2336.

Liu, L., and Duff, K. (2008). A technique for serial collection of cerebrospinal fluid from the cisterna magna in mouse. J. Vis. Exp. http://dx.doi.org/10.3791/960.

Lowry, O.H., Rosebrough, N.J., Farr, A.L., and Randall, R.J. (1951). Protein measurement with the Folin phenol reagent. J. Biol. Chem. *193*, 265–275.

Ma, Y., Chapman, J., Levine, M., Polireddy, K., Drisko, J., and Chen, Q. (2014). High-dose parenteral ascorbate enhanced chemosensitivity of ovarian cancer and reduced toxicity of chemotherapy. Sci. Transl. Med. *6*, 222ra18.

Macdonald, D.R., Cascino, T.L., Schold, S.C., and Cairncross, J.G. (1990). Response criteria for phase II studies of supratentorial malignant glioma. J. Clin. Oncol. *8*, 1277–1280.

Matsubara, D., Kishaba, Y., Ishikawa, S., Sakatani, T., Oguni, S., Tamura, T., Hoshino, H., Sugiyama, Y., Endo, S., Murakami, Y., et al. (2013). Lung cancer with loss of BRG1/BRM, shows epithelial mesenchymal transition phenotype and distinct histologic and genetic features. Cancer Sci. *104*, 266–273.

Moertel, C.G., Fleming, T.R., Creagan, E.T., Rubin, J., O'Connell, M.J., and Ames, M.M. (1985). High-dose vitamin C versus placebo in the treatment of patients with advanced cancer who have had no prior chemotherapy. A randomized double-blind comparison. N. Engl. J. Med. *312*, 137–141.

Mojić, M., Bogdanović Pristov, J., Maksimović-Ivanić, D., Jones, D.R., Stanić, M., Mijatović, S., and Spasojević, I. (2014). Extracellular iron diminishes anticancer effects of vitamin C: an in vitro study. Sci. Rep. *4*, 5955.

Monti, D.A., Mitchell, E., Bazzan, A.J., Littman, S., Zabrecky, G., Yeo, C.J., Pillai, M.V., Newberg, A.B., Deshmukh, S., and Levine, M. (2012). Phase I evaluation of intravenous ascorbic acid in combination with gemcitabine and erlotinib in patients with metastatic pancreatic cancer. PLoS One *7*, e29794.

Moser, J.C., Rawal, M., Wagner, B.A., Du, J., Cullen, J.J., and Buettner, G.R. (2014). Pharmacological ascorbate and ionizing radiation (IR) increase labile iron in pancreatic cancer. Redox Biol. *2*, 22–27.

Nath, K.A., Ngo, E.O., Hebbel, R.P., Croatt, A.J., Zhou, B., and Nutter, L.M. (1995). alpha-Ketoacids scavenge $H_2O_2$ in vitro and in vivo and reduce menadione-induced DNA injury and cytotoxicity. Am. J. Physiol. *268*, C227–C236.

Oberley, L.W., Oberley, T.D., and Buettner, G.R. (1980). Cell differentiation, aging and cancer: the possible roles of superoxide and superoxide dismutases. Med. Hypotheses *6*, 249–268.

Olney, K.E., Du, J., van 't Erve, T.J., Witmer, J.R., Sibenaller, Z.A., Wagner, B.A., Buettner, G.R., and Cullen, J.J. (2013). Inhibitors of hydroperoxide metabolism enhance ascorbate-induced cytotoxicity. Free Radic. Res. *47*, 154–163.

Ornstein, L. (1964). Disc electrophoresis I. Background and theory. Ann. N. Y. Acad. Sci. *121*, 321–349.

Packer, L., and Fuehr, K. (1977). Low oxygen concentration extends the lifespan of cultured human diploid cells. Nature *267*, 423–425.

Padayatty, S.J., Sun, H., Wang, Y., Riordan, H.D., Hewitt, S.M., Katz, A., Wesley, R.A., and Levine, M. (2004). Vitamin C pharmacokinetics: implications for oral and intravenous use. Ann. Intern. Med. *140*, 533–537.

Pantopoulos, K., Mueller, S., Atzberger, A., Ansorge, W., Stremmel, W., and Hentze, M.W. (1997). Differences in the regulation of iron regulatory protein-1 (IRP-1) by extra- and intracellular oxidative stress. J. Biol. Chem. *272*, 9802–9808.

Riordan, N.H., Riordan, H.D., Meng, X., Li, Y., and Jackson, J.A. (1995). Intravenous ascorbate as a tumor cytotoxic chemotherapeutic agent. Med. Hypotheses *44*, 207–213.

Rumsey, S.C., Kwon, O., Xu, G.W., Burant, C.F., Simpson, I., and Levine, M. (1997). Glucose transporter isoforms GLUT1 and GLUT3 transport dehydroascorbic acid. J. Biol. Chem. *272*, 18982–18989.

Sandler, A., Gray, R., Perry, M.C., Brahmer, J., Schiller, J.H., Dowlati, A., Lilenbaum, R., and Johnson, D.H. (2006). Paclitaxel-carboplatin alone or with bevacizumab for non-small-cell lung cancer. N. Engl. J. Med. *355*, 2542–2550.

Schiller, J.H., Harrington, D., Belani, C.P., Langer, C., Sandler, A., Krook, J., Zhu, J., Johnson, D.H., and Eastern Cooperative Oncology Group. (2002). Comparison of four chemotherapy regimens for advanced non-small-cell lung cancer. N. Engl. J. Med. *346*, 92–98.

Simon, R., Freidlin, B., Rubinstein, L., Arbuck, S.G., Collins, J., and Christian, M.C. (1997). Accelerated titration designs for phase I clinical trials in oncology. J. Natl. Cancer Inst. *89*, 1138–1147.

Spitz, D.R., and Oberley, L.W. (2001). Measurement of MnSOD and CuZnSOD activity in mammalian tissue homogenates. Curr. Protoc. Toxicol. *Chapter 7*. Unit 7.5.

Spitz, D.R., Dewey, W.C., and Li, G.C. (1987). Hydrogen peroxide or heat shock induces resistance to hydrogen peroxide in Chinese hamster fibroblasts. J. Cell. Physiol *131*, 364–373.

Spitz, D.R., Sim, J.E., Ridnour, L.A., Galoforo, S.S., and Lee, Y.J. (2000). Glucose deprivation-induced oxidative stress in human tumor cells. A fundamental defect in metabolism? Ann. N. Y. Acad. Sci. *899*, 349–362.

Springer, E.L. (1980). Comparative study of the cytoplasmic organelles of epithelial cell lines derived from Hu man carcinomas and nonmalignant tissues. Cancer Res. *40*, 803–817.

Storer, B.E. (1989). Design and analysis of phase I clinical trials. Biometrics *45*, 925–937.

Stupp, R., Mason, W.P., van den Bent, M.J., Weller, M., Fisher, B., Taphoorn, M.J.B., Belanger, K., Brandes, A.A., Marosi, C., Bogdahn, U., et al. (2005). Radiotherapy plus concomitant and adjuvant temozolomide for glioblastoma. N. Engl. J. Med. *352*, 987–996.

Sunaga, N., Shames, D.S., Girard, L., Peyton, M., Larsen, J.E., Imai, H., Soh, J., Sato, M., Yanagitani, N., Kaira, K., et al. (2011). Knockdown of oncogenic KRAS in non-small cell lung cancers suppresses tumor growth and sensitizes tumor cells to targeted therapy. Mol. Cancer Ther. *10*, 336–346.

Szatrowski, T.P., and Nathan, C.F. (1991). Production of large amounts of hydrogen peroxide by human tumor cells. Cancer Res. *51*, 794–798.

Torti, S.V., and Torti, F.M. (2013). Iron and cancer: more ore to be mined. Nat. Rev. Cancer *13*, 342–355.

Ueda, M., Toji, E., Nunobiki, O., Izuma, S., Okamoto, Y., Torii, K., and Noda, S. (2008). Mutational analysis of the BRAF gene in human tumor cells. Hum. Cell *21*, 13–17.

Verrax, J., and Calderon, P.B. (2009). Pharmacologic concentrations of ascorbate are achieved by parenteral administration and exhibit antitumoral effects. Free Radic. Biol. Med. *47*, 32–40.

Vislisel, J.M., Schafer, F.Q., and Buettner, G.R. (2007). A simple and sensitive assay for ascorbate using a plate reader. Anal. Biochem. *365*, 31–39.

Welsh, J.L., Wagner, B.A., van't Erve, T.J., Zehr, P.S., Berg, D.J., Halfdanarson, T.R., Yee, N.S., Bodeker, K.L., Du, J., Roberts, L.J., 2nd, et al. (2013). Pharmacological ascorbate with gemcitabine for the control of metastatic and node-positive pancreatic cancer (PACMAN): results from a phase I clinical trial. Cancer Chemother. Pharmacol. *71*, 765–775.

Witmer, J.R., Wetherell, B.J., Wagner, B.A., Du, J., Cullen, J.J., and Buettner, G.R. (2016). Direct spectrophotometric measurement of supra-physiological levels of ascorbate in plasma. Redox Biol. *8*, 298–304.

Yun, J., Mullarky, E., Lu, C., Bosch, K.N., Kavalier, A., Rivera, K., Roper, J., Chio, I.I.C., Giannopoulou, E.G., Rago, C., et al. (2015). Vitamin C selectively kills KRAS and BRAF mutant colorectal cancer cells by targeting GAPDH. Science *350*, 1391–1396.

Zwacka, R.M., Dudus, L., Epperly, M.W., Greenberger, J.S., and Engelhardt, J.F. (1998). Redox gene therapy protects human IB-3 lung epithelial cells against ionizing radiation-induced apoptosis. Hum. Gene Ther. *9*, 1381–1386.

# STAR★METHODS

## KEY RESOURCES TABLE

| REAGENT or RESOURCE | SOURCE | IDENTIFIER |
|---|---|---|
| Antibodies | | |
| Anti-β-Actin | Sigma-Aldrich, Inc. | RRID: AB_476697 |
| Anti-ferritin heavy chain | Abcam, Cambridge, MA | RRID: AB_1310223 |
| Anti-ferritin light chain | Abcam, Cambridge, MA | RRID: AB_10862715 |
| Anti-mouse IgG | Sigma-Aldrich, Inc. | RRID: AB_258264 |
| Anti-rabbit IgG | Sigma-Aldrich, Inc. | RRID: AB_258207 |
| Anti-Transferrin Receptor | Invitrogen/Thermo Scientific | RRID: AB_2533029 |
| Bacterial and Virus Strains | | |
| AdCatalase (AdCat) | ViraQuest, Inc. | VQAd CMV hCatalase |
| AdGlutathione Peroxidase 1 (AdGPx1) | ViraQuest, Inc. | VQAd CMV GPX "D1" |
| AdSOD1 | ViraQuest, Inc. | VQAd CMV hCuZnSOD |
| AdSOD2 | ViraQuest, Inc. | VQAd CMVhMnSOD |
| AdEmpty (AdE) | ViraQuest, Inc. | VQAd Empty |
| AdFerritin Heavy Chain (AdFtH) | ViraQuest, Inc. | VQAd FTH1 |
| AdFerritin Light Chain (AdFtL) | ViraQuest, Inc. | VQAd FTL |
| Chemicals, Peptides, and Recombinant Proteins | | |
| $^{14}$C-EDTA | American Radiolabeled Chemicals, Inc. | Catalog # ARC 392 |
| dehydroascorbate (DHA) | Sigma-Aldrich, Inc. | CAS# 113170-55-1 |
| GC4419 | Gift from Galera Therapeutics, Inc., Malvern, PA | N/A |
| L-ascorbic acid | Macron Chemicals/Avantor | CAS# 50-81-7 |
| L-ascorbic acid (clinical) | Mylan Institutional, LLC | NDC# 67457-118-50 |
| L-ascorbic acid (clinical) | McGuff Pharmaceuticals, Inc. | Item # 008232 |
| Experimental Models: Cell Lines | | |
| A549 | American Type Culture Collection | RRID: CVCL_0023 |
| H1299 | American Type Culture Collection | RRID: CVCL_0060 |
| H23 | American Type Culture Collection | RRID: CVCL_1547 |
| H292 | American Type Culture Collection | RRID: CVCL_0455 |
| HBEpC | Cell Applications, Inc. | Catalog # 502-05a |
| HEL. 92.1.7 | American Type Culture Collection | RRID: CVCL_2481 |
| NHA | Lonza Walkersville, Inc. | Catalog # CC-2565 |
| U118 | American Type Culture Collection | RRID: CVCL_0633 |
| U251 | Sigma-Aldrich, Inc. | RRID: CVCL_0021 |
| U87 | American Type Culture Collection | RRID: CVCL_0022 |
| Experimental Models: Organisms/Strains | | |
| Athymic *Foxn1$^{nu}$/Foxn1$^{nu}$* | Envigo (Formerly Harlan Laboratories) | N/A |
| Oligonucleotides | | |
| Silencer® Select Negative Control No. 1 | Ambion, ThermoFisher Scientific | Catalog # 4390844 |
| Silencer® Select siRNA TFRC (s727) | Ambion, ThermoFisher Scientific | Catalog # 4390826 |

## CONTACT FOR REAGENT AND RESOURCE SHARING

Further information and requests for resources and reagents should be directed to and will be fulfilled by the Lead Contact, Douglas R. Spitz (douglas-spitz@uiowa.edu).

## EXPERIMENTAL MODEL AND SUBJECT DETAILS

### Cell Lines and Primary Cultures

NSCLC cell lines H292 (source: female), H1299 (source: male), H23 (source: male), and A549 (source: male) and HEL 92.1.7 cells (source: male) were grown in RPMI 1640 medium supplemented with 10% fetal bovine serum (FBS). Normal human bronchial epithelial cells (HBEpC) were gown in proprietary HBE medium and growth supplements (Cell Applications, Inc). HBEpCs from both a male and female source were utilized in this manuscript. GBM cell lines U87 (source: male), U118 (source: male), U251 (source: male), and normal human astrocytes (NHA) (sources: two male cultures) were grown in DMEM F12 medium supplemented with 15% FBS, 10 $\mu g\ mL^{-1}$ insulin, 7.5 $ng\ mL^{-1}$ fibroblast growth factor (FGF), 1 mM sodium pyruvate, 15 mM HEPES buffer (pH 7.2), and 100 units/100 $\mu g\ mL^{-1}$ penicillin/streptomycin.

As primary cells in culture grow better under normoxic conditions (4% $O_2$) (Packer and Fuehr, 1977) and this manuscript investigates intrinsic differences between cancer and primary cells, all cells were incubated at 4% $O_2$ in a humidity controlled environment (37 °C, 5% $CO_2$; Forma Scientific). Importantly, we did not see any difference in toxicity in cancer cells exposed to ascorbate for 1 hr in 21% or 4% $O_2$ (data not shown). In all experiments utilizing HEL 92.1.7 and A549 parental and $SOD2^{-/-}$ cells, cells were maintained and experiments were performed at 21% $O_2$ to maximize effects on superoxide production. All cell lines were utilized before passage 20 and treated in exponential growth phase at 50-75% confluence. Doubling times of HBEpCs and NHAs were monitored and cells were utilized until doubling time increased by 50%.

### In Vivo Mouse Studies

Female 4-6 week old athymic nude mice (*Foxn1*$^{nu}$/*Foxn1*$^{nu}$) were purchased from Envigo (previously Harlan Laboratories) and housed in the Animal Care Facility at The University of Iowa (Iowa City, IA), and all procedures were approved by The University of Iowa Institutional Animal Care and Use Committee and conformed to NIH guidelines. All mice were treatment naïve at the time of tumor cell introduction. For all xenograft studies, after tumors were established, mice were randomly assigned to experimental groups. Mouse weights throughout the experiments are illustrated in Figure 2C.

### Clinical Trials

For the phase I clinical trial evaluating the safety of combining pharmacological ascorbate with standard radiation and temozolomide in glioblastoma (GBM) patients, approval was sought, and obtained, from The University of Iowa Institutional Review Board (Biomedical IRB-01; IRB 201211713). For the phase II clinical evaluating the efficacy of combining carboplatin and paclitaxel with pharmacological ascorbate in advanced stage (stage IIIB and IV) NSCLC patients, approval was sought, and obtained, from The University of Iowa Institutional Review Board (Biomedical IRB-01; IRB 201412760). Both trials were registered with clinicaltrials.gov prior to enrollment of the first subject (NCT01752491 and NCT02420314, respectively). Both clinical trials were conducted compliant with good clinical practice, including obtaining informed consent directly from all trial participants; none of the elements of consent were waived.

## METHOD DETAILS

### Ascorbate and Ascorbate Exposure

L-Ascorbic acid stock solution (approx. 1 M) was made in Nanopure® Type 1 water (18 MΩ) with the pH adjusted to 7.0 with 1 M NaOH, stored in sealed glass tubes with minimal head space, and the precise concentration was confirmed spectrophotometrically as previously described (265 nm, $\varepsilon = 14.5\ mM^{-1}\ cm^{-1}$) (Buettner, 1988). For all experiments directly comparing the effects of ascorbate on cancer and normal cells, ascorbate is dosed per cell due to previous literature demonstrating that $H_2O_2$ and ascorbate toxicity is dependent on cell number/density (Doskey et al., 2015; Spitz et al., 1987). Furthermore, the media conditions, including media volume, during cancer vs. normal comparisons are identical, as media constitution (i.e. serum, pyruvate and other $\alpha$-ketoacids, metal ions, etc.) and media pH (i.e. lactate production) modulate ascorbate toxicity and can account for apparent differences in cell sensitivity to ascorbate within a given cell type (Buettner, 1988; Spitz et al., 1987; Olney et al., 2013; Nath et al., 1995; Clément et al., 2001; Mojić et al., 2014). For NSCLC and HBEpC comparisons, cells were exposed to ascorbate in serum-free RPMI supplemented with HBE media supplements and returned to their normal maintenance media for cloning. For clinical dosing, the studies utilize commercially available, prescription-only L-ascorbic acid for intravenous injection (500 $mg\ mL^{-1}$).

Although the data investigating tissue ascorbate concentrations following pharmacological ascorbate administration is limited, initial measurements of ascorbate levels in syngeneic mice bearing Lewis lung carcinoma tumors following 1 $g\ kg^{-1}$ IP ascorbate resulted in peak plasma concentrations of 4.7 ± 0.6 mM that resulted in peak tumor tissue homogenate concentrations of 1.04 $\mu moles\ g^{-1}$ wet weight (Campbell et al., 2016). This would convert to approximately 1.04 mM tissue concentrations assuming the wet weight of tissue is approximately the same as $_{H2O}$ (1 $g\ mL^{-1}$). In a different study when nude mice with 9L glioma xenografts were treated with 4 $g\ kg^{-1}$ ascorbate IP (Chen et al., 2008), peak tumor concentrations of >30 mM ascorbate were reported. Given these previous results, all in vitro ascorbate doses utilized in the current report (0.5-20 mM) are well within the range of likely ascorbate concentrations achieved in tumor and normal tissues in vivo (Campbell et al., 2016; Chen et al., 2008).

### Ionizing Radiation

Ionizing radiation (IR) was delivered in the Iowa Radiation and Free Radical Research Core facility using a Pantak Therapx DXT 300 X-ray machine operated at 200 kVp with added filtration of 0.35 mm Cu + 1.5 mm Al, resulting in a beam quality of 0.95 mm Cu. For in vitro studies, cells were irradiated in 60 mm cell culture dishes. For in vivo murine xenograft studies, mice were anesthetized using an 87.5 mg $kg^{-1}$ ketamine and 12.5 mg $kg^{-1}$ xylazine mixture and placed in lead boxes with only their right flank exposed.

### Clonogenic Survival, Viability, and Metabolic Activity Assays

Cells (1-2 x $10^5$) were plated in 60 mm cell culture dishes and grown in their respective media for 48 hr before exposed to experimental conditions. For radio-chemotherapy sensitization experiments, the cells were sequentially exposed to 1 h chemotherapy, 1 h pharmacological ascorbate, and then 2 Gy IR. For bovine catalase experiments, catalase was added 1 min prior to ascorbate exposure. For AdGPx1 experiments, cells were supplemented with 30 nM sodium selenite following transduction and throughout clonogenic growth. For iron chelation or iron addition experiments, chelators were added 3 hr prior to and during ascorbate exposure to ensure that labile metal ions were sufficiently bound. For experiments investigating the role of intracellular versus extracellular iron, chelators were either added 3 h prior to ascorbate exposure and washed before ascorbate exposure, or media that was to be added later during ascorbate exposure was pre-chelated for 3 hr at 37 °C. For experiments testing the ability of AntA to sensitize NHAs to ascorbate, trypsinized NHAs were exposed in solution to 25 μM AntA in the presence or absence of 10 pmol $cell^{-1}$ (2 mM) $AscH^-$ prior to flow cytometry or clonogenic cell survival analysis. For 2-DG experiments, 20 mM 2-DG was added only 15 min prior to ascorbate exposure to ensure minimal 2-DG-mediated effect of cellular redox potential. For the comparison of the toxicity of $AscH^-$ vs. DHA, DHA was dissolved in acetate buffer (pH 5) prior to exposure and equivalent acetate buffer was added to control cultures ($[]_{final}$ = 3.15 mM).

After treatment, cells were washed with PBS and clonogenic assay was completed in their respective media. Briefly, floating and attached cells were collected and total cells per plate were counted. An experimentally derived number of cells were plated into each well of a 6-well cell culture plate in their respective media. For HEL92.1.7 suspension cells, cells were seeded in a top layer of 0.4% (w/v) agarose to allow for quantifiable colony formation. After sufficient time (7-12 days, cell type-dependent), cells were fixed in 70% ethanol and stained with a Brilliant Blue methanol solution. Cell colonies containing greater than 50 cells were counted and utilized to calculate plating efficiency for each treatment group. Normalized survival fractions were calculated by comparing plating efficiencies of each treatment group against the control group within a given experiment.

Trypan blue viability assay was performed immediately after 1 hr exposure to ascorbate on a Countess™ Automated Cell Counter (Invitrogen) as per the accompanying manufacturer's protocol and normalized to control untreated cells.

Resazurin (*a.k.a.* Alamar Blue) was utilized to assess metabolic activity. Following 1 hr exposure to ascorbate, cells were washed, and stained in 6 μM resazurin for 1.5 h at 37 °C. Cells were then washed twice in PBS, trypsinized, and spun at 1200 rpm x 5 min. Pellets were resuspended in PBS and 10,000 cells were assayed for the reduction of resazurin (non-fluorescent) to resorufin (fluorescent) and analyzed on a LSR II Flow Cytometer (BD Biosciences; $\lambda_{ex}$ = 561 nm, $\lambda_{em}$ = 582/15 nm).

### Murine Xenograft Models

1 x $10^6$ H292 or U87 cells were injected subcutaneously into the right rear flank. Once tumors were established, treatment was initiated with daily ascorbate (4 g $kg^{-1}$ or equivalent dose of NaCl, IP), weekly carboplatin (5 mg $kg^{-1}$ for H292) or temozolomide (2.5 mg $kg^{-1}$ for U87), and/or IR (12 Gy/ 2 frx). Ascorbate/NaCl and chemotherapy was continued for the full extent of the study. Tumors were measured every other day with Vernier calipers (volume = (length x width x (width/2)) and mice were euthanized and sacrificed when tumor length exceeded 1.5 cm in any dimension.

### Ascorbate Quantification

Tumor xenografts were excised and flash frozen in liquid nitrogen until analysis. Cell culture lysates were collected, and immediately assayed for ascorbate concentration. Mouse whole blood was collected by cardiac puncture, and plasma was collected after the sample was centrifuged at 500 g for 10 min and frozen until analysis. For patient samples, whole blood was collected from clinical trial patients (NaHeparin 75 USP units, BD Vacutainer® green top blood collection tube, 4 mL), and plasma was collected after centrifugation at 500 g for 10 min and aliquoted and stored at -80 °C until analysis.

Total ascorbate in cell culture lysates, mouse samples, and GBM subjects was quantified as previously described (Vislisel et al., 2007; Welsh et al., 2013). Briefly, samples were extracted in a buffer containing 90% methanol and 10% water with 250 μM DETAPAC (90:10, v/v), mixed, and incubated on ice for 10 min to precipitate protein. The samples were clarified by centrifugation (16 g, 10 min) with an Eppendorf model 5415D Microfuge. Specifically, samples were diluted at a ratio of 50 μL of plasma to 450 μL extraction buffer. These samples were then further diluted another 77.5 to 105-fold (therefore, 775 to 1,050 fold overall) in a buffer containing 72% methanol and 28% water with 250 μM DETAPAC (72:28, v/v). L-ascorbic acid standards were prepared in 72% methanol and 28% water with 250 μM DETAPAC (72:28, v/v) with stock solution concentrations ranging from 2.5 to 50 μM. This protocol ensured that all samples had identical methanol content which is critical for accurate quantification (Vislisel et al., 2007).

Aliquots (100 μL) of the samples or standards were placed in 96-well optical bottom black plates (Thermo Fisher Scientific, Rochester, NY, USA). The assay was initiated at room temperature by adding 100 μL of 2.3 mM 4-hydroxy-2,2,6,6-tetramethylpiperidinyloxyl (Tempol) in 2 M sodium acetate trihydrate buffer previously adjusted to pH 5.5 with acetic acid. The samples were then incubated for 10 min in the dark, allowing for Tempol-mediated oxidation of ascorbate to dehydroascorbate (DHA). Subsequently, 42 μL of 5.5 mM ortho-phenylenediamine (oPDA) in 2 M sodium acetate buffer (pH 5.5) was added to the samples. Kinetic measurements were

immediately initiated and collected every 22 s using a TECAN SpectraFluor Plus plate reader (Tecan, Research Triangle Park, NC, USA) for the fluorescent condensation product of the reaction of oPDA with DHA (3-(dihydroxyethyl)furo[3,4-b]quinoxaline-1-one; $\lambda_{ex}$ = 345 nm, $\lambda_{em}$ = 425 nm). Plasma ascorbate concentrations were determined against the linear portions of the standard curve and corrected for previous dilutions.

Total ascorbate in NSCLC subject's plasma was quantified as previously described (Witmer et al., 2016). Briefly, plasma samples were measured spectrophotometrically (265 nm; $\varepsilon = 13{,}000\ M^{-1}\ cm^{-1}$) using an Implen Nanophotometer P-330 with a 250x dilution lid, path length = $4.00 \times 10^{-3}$ cm. The blank for each sample was a pair- 'pre-infusion' plasma sample, which allowed removal of the background absorbance of plasma proteins and other constituents.

### CSF Ascorbate Radical Electron Paramagnetic Resonance (EPR)

CSF was collected from nude athymic female mice that had received daily IP injections of ascorbate (4 g $kg^{-1}$) for two weeks as previously described (Liu and Duff, 2008). Briefly, mice were anesthetized (17.5 mg $ml^{-1}$ ketamine/2.5 mg $ml^{-1}$ xylazine mixture), restrained in a stereotaxic frame with an acute head angle, and the dura mater covering the foramen magnum was surgically exposed. CSF was collected by capillary action following minimal puncture of the dura mater and frozen until EPR analysis. Ascorbate radical EPR spectra were obtained by placing the capillary tube into the bottom of a 250 mm x 3 mm (ID) thin walled quartz EPR tube (707-SQ-250M Wilmad-Lab Glass, Vineland, NJ) centered in a Bruker HS EPR cavity (Bruker, Billerica, MA). Spectra of the ascorbate radical (g = 2.0052) were acquired by a Bruker EMX EPR spectrometer at room temperature while using a microwave power of 3.2 mW; frequency, 9.858 GHz; scanning 10 G with a sweep time of 20.972 s; receiver gain, $5.02 \times 10^4$; modulation frequency, 100 kHz; modulation amplitude, 0.70 G; signal channel time constant, 327.680 ms. Spectra were collected in the additive mode using 5 scans.

### Adenovirus Transduction

Replication-incompetent adenoviral vectors, Ad-empty (AdE), 25 MOI AdCMV catalase (AdCat), 25 MOI AdCMV glutathione peroxidase 1 (AdGPx1), 50 MOI AdCMV SOD1 (AdSOD1), and 50 MOI AdCMV SOD2 (AdSOD2) vectors are previously described (Zwacka et al., 1998; Ahmad et al., 2005, 2008). 20 MOI AdFerritin heavy and light chain (AdFtH and AdFtL, respectively) were generated by ViraQuest (North Liberty, IA) using commercially available iron regulatory element (IRE)-lacking vectors (OriGene). All transductions were performed in serum-free DMEM for 8-12 hr once cells reached 50-70% confluency. Cells were washed and grown in full media for an additional 36 hours before experiments were conducted. All transductions were confirmed by activity assay and/or western blot for each individual experiment.

### Radiolabeled $^{14}$C-EDTA Uptake

H292 NSCLC cells were exposed to 1 mM 'cold' EDTA spiked with $5 \times 10^5$ predicted disintegrations per minute (DPM) $^{14}$C-EDTA, which had a negligible effect on overall EDTA concentration, for 3 hr. To control for any effects of salt composition on radioactivity quantification, all sample vials contained 15 mL liquid scintillation cocktail + 5 mL of media, PBS, or trypsin. All samples were divided into 'media,' 'wash,', or 'cells' vials. The 'media' vial contained 4 mL spiked media + 1 mL PBS wash. The 'wash' vial contained 5 x 1 mL wash. The 'cells' vials contained 1 mL tyrpsin + H292 cells + 4 x 1 mL PBS washes. For the standard curve, all standards were added to 5 mL PBS + 15 mL liquid scintillation cocktail. All radioactive counts were collected on a liquid scintillation counter (Beckman #L2100) and fraction of EDTA in samples were calculated after subtraction of background counts:

$$[\mathrm{EDTA}]_{\mathrm{cellular}}\ (\mathrm{mM}) = \frac{\left(\frac{\mathrm{CPM\ (cells)}}{\mathrm{CPM\ (total)}}\right)\left(\frac{\mathrm{moles\ EDTA}}{\mathrm{plate}}\right)}{\mathrm{Total\ Cells} \times \mathrm{Cell\ Volume\ (L)}} \times \left(\frac{1000\ \mathrm{mmoles}}{1\ \mathrm{mole}}\right).$$

### Human Tissue Sample Collection and Inclusion Metrics

Tumor and adjacent normal was collected from patients with suspected or confirmed NSCLC patients through the IRB-approved University of Iowa Tissue Procurement Core and was frozen in Tissue-Tek® O.C.T. Compound. A board certified pathologist from the University of Iowa Hospital and Clinics histologically confirmed the NSCLC diagnosis. Samples were utilized for further studies if histology revealed >75% tumor or normal tissue, respectively, in adjacent tissue slices both before and after the samples were collected.

### Tissue DHE Staining and Quantification

From OCT-frozen patient tissue, 10 μm sections of both tumor and adjacent normal tissue were cut and placed on the same slide to control. Tissue sections were stained with 10 μM DHE for 30 min in PBS + 5 mM sodium pyruvate prior to analysis by confocal microscopy (Olympus FLUOVIEW FV1000). For treatment groups, tissue sections were pretreated for 30 min with 0.25 μM GC4419 SOD mimetic or, alternatively, as a positive control, tissue sections were co-treated with 10 μM antimycin A (AntA) during the last 15 min of DHE staining. Each image obtained was quantified by measuring the mean fluorescence intensity of at least 200 cell nuclei (ImageJ), and normalized to nuclei from untreated normal tissue cell nuclei.

To test the specificity of GC4419, any reaction with $H_2O_2$ was tested spectrophotometrically (240 nm; $\varepsilon$ = 39.4 $M^{-1}$ $cm^{-1}$) by measuring the disappearance of $H_2O_2$ in the presence of 0.25 μM GC4419 or 15 mkU $mL^{-1}$ bovine catalase in 50 mM phosphate buffer (pH 7.0).

### Tissue Iron Quantification

Labile iron in patient NSCLC and adjacent normal tissue was quantified as previously described (Moser et al., 2014). Wherever possible, metal instrumentation was avoided to prevent contamination from adventitious labile iron. Briefly, tissue sections were homogenized in a 1.5 mL eppendorf tube by plastic pestle in 350 μL PBS (pH 6.5) that was previously treated with Chelex® 100 beads to remove any adventitious labile iron. To this homogenate, 2 mM DFO (final concentration) was added and samples were incubated on ice for 1 hr and frozen at -80 °C until analysis. For analysis, samples were placed in 4 mm O.D. EPR tubes (Wilmad-LabGlass, Vineland, NJ, 707-SQ-250M) and were flash frozen in liquid nitrogen. The samples were then analyzed for labile iron by using EPR (Bruker EMX EPR spectrometer), monitoring for the high spin ferrioxamine ($Fe^{3+}$-DFO) signal at g = 4.3 at 100 K (Bruker ER4111VT variable temperature accessory) with the following EPR instrument parameters: center field 1575 G, sweep width 500 G, typical microwave frequency 9.766 GHz, power 20 mW, receiver gain 2 × $10^5$, modulation frequency 100 kHz, modulation amplitude 2 G, time constant 163.84 ms, conversion time 20.48 ms, resolution 1024 points, and with 5 additive scans. All samples were analyzed three times, repositioning the sample in the cavity before initiating each additional scan. The mean signal intensity was quantified and the labile iron content was calculated using a standard curve (0 – 15 μM FAS with 1 mM DFO) and normalized to total tissue protein by the Pierce™ BCA protein assay kit (Thermo Fisher Scientific), which is not susceptible to interference from residual OCT as opposed to the Lowry method (data not shown). Furthermore, equimolar DFO was added into the standard curve to control for any potential interference of DFO in the assay system (data not shown).

### CRISPR/Cas9-Mediated Deletion of SOD2

The CRISPR/Cas9 system was utilized to delete mitochondrial SOD2 from A549 and HEL 92.1.7 cells as previously described in HEK293T cells (Cramer-Morales et al., 2015). Briefly, cells were electroporated (200 V, 30 μF) with the custom synthesized pD130-GFP expression vector containing expression cassettes for GFP (GFP), Cas9 endonuclease, and a CRISPR chimeric cDNA with a gRNA moiety designed to target SOD2 (DNA 2.0, Menlo Park, CA). Cells that transiently expressed GFP were sorted by flow cytometry and cloned. Deletion of SOD2 was confirmed by western blot and activity assays (Figure S5).

### SOD Activity Assay

MnSOD activity was measured in cell lysates as previously described (Spitz and Oberley, 2001). Briefly, dry cell pellets were homogenized in 50 mM phosphate buffer with 1.34 mM DETAPAC. To measure MnSOD activity only, the sample is incubated with 5 mM $NaCN^-$ for 30 min to inhibit CuZnSOD activity. To measure the MnSOD activity, the rate of nitroblue tetrazolium (NBT) reduction was measured during the reaction of 100 μL of increasing amounts of total sample protein (0 – 500 mg), 100 μL of $10^{-2}$ U $mL^{-1}$ xanthine oxidase, and 800 μL of 50 mM phosphate buffer (1 mM DETAPAC, 0.13 mg $mL^{-1}$ BSA, 1.0 U $mL^{-1}$ catalase, 5.6 x $10^{-5}$ M NBT, 1 x $10^{-4}$ M xanthine, 5 mM $NaCN^-$, 50 μM bathocuproine disulfonic acid) at 560 nm for 2 min. One unit of SOD activity is measured as the amount of protein necessary to reach 50% of maximum inhibition of NBT reduction.

To account for incomplete $CN^-$- mediated inhibition of CuZnSOD activity, MnSOD and CuZnSOD activity was more specifically differentiated by a SOD activity gel as adapted from techniques previously described (Ornstein, 1964). Briefly, a 12% polyacrylamide gel was made and pre-electrophoresed for 1 hr at 40 A (188 mM Tris-base, 1.3 mM EDTA, pH 8.8). The following day, a 5% polyacrylamide stacking gel with 0.004% riboflavin-5'-phosphate with a 1.5 mm comb was solidified under a fluorescent light for 15 – 30 min. 100 μg total protein was electrophoresed for approximately 3 hr at 40 A (50 mM Tris base, 300 mM glycine, 2.3 mM EDTA, pH 8.3) while the gel electrophoresis box was placed in a ice bath to maintain protein activity. The gels were then soaked in the staining solution (2.43 mM NBT, 28 mM TEMED, 2.8 x $10^{-5}$ M riboflavin-5'-phosphate in $ddH_2O$) for 20 min at room temperature in the dark. The gels were then rinsed, placed in 50 mM phosphate buffer (pH 7.8) and exposed to fluorescent light to initiate superoxide production. Achromatic bands indicate the presence of SOD activity. Once developed, the gels were further developed at room temperature overnight and imaged.

### Cellular Labile Iron Pool Quantification

The labile iron pool (LIP) was visualized using the fluorescent dye Calcein-AM as previously described with modifications (Epsztejn et al., 1997). Briefly, after sample treatment, cells were trypsinized, spun at 1,200 rpm for 5 min, and resuspended at approximately 1 x $10^6$ cells $mL^{-1}$ in 500 nM Calcein-AM in PBS. Samples were incubated for 15 min at 4% $O_2$ in a humidity controlled environment (37 °C, 5% $CO_2$). Subsequently, samples were pelleted, washed in PBS, and resuspended in 1 mL PBS before dividing each sample into two flow cytometry sample tubes, to which 100 μM 2',2'-bipyridyl (BIP) was added to one tube. Samples were kept at room temperature and 10,000 cells were analyzed on a LSR II Flow Cytometer (BD Biosciences; $\lambda_{ex}$ = 488 nm, $\lambda_{em}$ = 515/20 nm). BIP tubes were incubated for at least 15 minutes before analysis to allow for full chelation of intracellular labile iron. The LIP (A.U.) = $MFI_{BIP}$ – $MFI_{NoBIP}$ was normalized against the control samples to calculate the relative labile iron pool.

To determine any interaction with ascorbate, BIP-mediated change in calcein fluorescence (100 nM Calcein; 20 nM FAS) was measured in Luminescence Spectrometer LS 50B (PerkinElmer) in the presence or absence of 5 mM ascorbate after incubation at 37 °C for 20, 40, or 60 min.

### Western Blots

Exponentially growing cells were washed with PBS before the addition of lysis buffer (Cell Signaling), incubated on ice for 5 minutes, and scraped. The lysate was collected and centrifuged to remove cellular debris. The protein concentrations were determined on the cleared lysate using the Bio-Rad DC Bradford Protein Assay (Bio-Rad Laboratories, Hercules, CA. Total protein (25μg) was electrophoresed on a 4-20% gradient gel (Bio-Rad) at 80 V for approximately 1 hr. The separated proteins were transferred onto PVDF membrane (Millipore, Billerica, CA) and non-specific binding was blocked using 5% nonfat dry milk in PBS-Tween (0.2%) for 1 hr at room temperature. The membranes were incubated with primary antibodies (Ferritin heavy chain, 1:1000, Ferritin light chain 1:10,000, both antibodies from Abcam, Cambridge, MA, Transferrin receptor, 1:1000, Invitrogen, Camarillo, CA) at 4° C overnight. Actin served as a loading control (1:4,000; Sigma-Aldrich). Following 3 x 5 min PBS-Tween washes, the membranes were blotted with secondary antibodies (1:25,000; Sigma-Aldrich, St. Louis, MO) that were conjugated with horseradish peroxidase for 1 hour. The washed membranes were incubated with Super Signal West Pico Chemiluminescent Substrate (Thermo Scientific, Rockford, IL) and exposed to CareStream BioMax MR Film (CareStream Health, Rochester, NY). Quantification of western blots were performed in ImageJ.

### Transferrin Receptor siRNA

For siRNA-mediated knockdown of TfR, we utilized a commercially available pre-validated siRNA construct (s727, Silencer® Select; Ambion, Life Technologies, Thermo Fisher Scientific) as well as a scrambled siRNA transfection control (Silencer® Select Negative Control No. 1). Cells were plated and allowed to grow 36-48 hr until they reached 30-40% confluence. siRNA (25 pmol per dish) and Lipofectamine® 2000 (10 μL per dish) were prepared as instructed in OptiMEM transfection media (Gibco). A master mix of siRNA (25 pmol per dish) and lipofectamine (10 μL per dish) were individual diluted in 500 μL OptiMEM per dish and allowed to incubate for 5 min at room temperature. These solutions were then combined, mixed gently, and allowed to incubate for an additional 20 min before adding 1 mL of the solution to each washed cell culture dish. The cells were exposed to the transfection medium for 8 – 12 hr, washed, and grown in full media until 80 – 90% confluence (~36 hr). Further experiments were conducted as described above. Because TfR mRNA is mostly regulated post-transcriptionally, and our endpoint was knockdown of TfR, knockdown in each experiment was confirmed by western blot of immune-reactive TfR protein (representative image: Figure 4M)

### Aconitase Activity

Exponentially growing cells were scraped and frozen as dry pellets until assayed for total aconitase activity adapted from as previously described (Case et al., 2011). Briefly, cell pellets were resuspended in 50 mM Tris-HCl, pH 7.4 with 0.6 mM $MnCl_2$ and 5 mM Na-citrate and sonicated 3 x 10 s each. Protein was quantified by the Lowry method (Lowry et al., 1951). Aconitase activity was measured as the rate of appearance of NADPH (at 340 nm; Beckman DU 800 spectrophotometer, Brea, CA) for 45 min during the reaction of 200 μg total sample protein with 200 μM $NADP^+$ and 10 U isocitrate dehydrogenase.

### ETC Complex Activity

Exponentially growing cells were scraped and frozen as dry pellets until assayed for protein content (Lowry) and maximal ETC complex activity as previously described (Birch-Machin et al., 1994). Briefly, dry cell pellets were resuspended in 20 mM potassium phosphate buffer and sonicated 3 x 10 s each. Rates of activities were normalized to total protein. Complex I activity was quantified as the rate of rotenone-inhibitable NADH oxidation (320 nm; $\varepsilon = 6.22\ mM^{-1}\ cm^{-1}$). Samples were assayed in the presence or absence of 200 μg $mL^{-1}$ rotenone in 25 mM potassium phosphate working buffer (5 mM $MgCl_2$, 2 mM KCN, 2.5 mg $mL^{-1}$ BSA, 0.13 mM NADH, 200 μg $mL^{-1}$ antimycin A, 7.5 mM coenzyme $Q_1$). Complex II activity was measured in the presence and absence of 0.2 M succinate in 25 mM potassium phosphate working buffer (5 mM $MgCl_2$, 2 mM KCN, 2.5 mg $mL^{-1}$ BSA for 10 minutes at 30 C. After incubation, 200 μg $mL^{-1}$ antimycin A, 200 μg $mL^{-1}$ rotenone, 5 mM 2,6-dichloroindophenol (DCIP), and 7.5 mM coenzyme $Q_1$ were added to each cuvette and incubated for 1 min before quantifying Complex II activity as the difference in the rate of DCIP reduction in the presence and absence of succinate (at 600 nm; $\varepsilon = 19.1\ mM^{-1}\ cm^{-1}$). Complex IV activity was assayed as the rate of oxidation of cytochrome c (500 nm; $\varepsilon = 19.6\ mM^{-1}\ cm^{-1}$). Whole cell lysates were assayed in 25 mM potassium phosphate buffer (0.5 mM n-dodecyl β-maltoside, 1.5 mM reduced cytochrome c).

### Quantification of Intracellular $H_2O_2$ with PeroxyOrange-1

To visualize intracellular $H_2O_2$ levels, the selectively sensitive fluorescent probe PeroxyOrange-1 was utilized as previously described with modifications (Dickinson et al., 2010). 1 x $10^5$ cells were plated and grown in their respective media for 48 hr. The complete protocol was conducted in the dark with minimal ambient lighting. Cells were washed with PBS and incubated with 10 uM PO-1 in phenol red free RPMI supplemented with HBE growth supplements for 1 hr at 37 °C. Cells were then washed in PBS and placed back in phenol red free RPMI supplemented with HBE growth supplements. At this time, treatment with 15 pmol $cell^{-1}$ ascorbate or 100 μM $H_2O_2$ (every 30 min) was initiated and cells were placed back at 37 °C. At times indicated, cells were placed on ice for the remainder of the protocol, washed, and trypsinized with phenol red free 0.5% trypsin. After 15 min, cells still attached were scraped and all cells were collected in 15 mL conical vials containing PBS + 10% FBS to neutralize the trypsin reaction. Cells were spun at 1200 rpm for 5 min at 4 °C, resuspended in 300-500 uL PBS and 10,000 cells were analyzed on a LSR II Flow Cytometer (BD Biosciences) with $\lambda_{ex}$=561nm, $\lambda_{em}$=585/20nm. The mean fluorescence intensity (MFI) was analyzed (FlowJo™) and corrected for autofluorescence against unlabeled cells. Normalized MFI was calculated by comparing MFI for a given treatment group against control.

To determine any interaction with ascorbate PO-1 fluorescence (10 μM PO-1, 100 μM $H_2O_2$) was measured in Luminescence Spectrometer LS 50B (PerkinElmer) in the presence or absence of 1 mM ascorbate.

### Phase I Clinical Trial of Pharmacological Ascorbate in Combination with Chemoradiation in GBM

A phase 1 clinical trial was conducted at the University of Hospitals and Clinics to evaluate the safety of combining pharmacological ascorbate with standard radiation and temozolomide in glioblastoma (GBM) patients. Approval was sought, and obtained, from the University of Iowa Institutional Review Board (Biomedical IRB-01; IRB 201211713). This phase 1 study was registered with clinicaltrials.gov (NCT 01752491) prior to enrollment of the first subject. Newly diagnosed GBM patients referred for standard therapy (Stupp et al., 2005) were invited to participate. Post-consent screening procedures included evaluating for glucose-6-phosphatase dehydrogenase deficiency as well as osmolarity tolerance by challenging the consented subjects with a 15 g ascorbate infusion.

The study was broken into two phases: radiation phase and adjuvant phase. Radiation phase was defined as the time period from day 1 of radiation through adjuvant cycle 1, day 1. Doses of pharmacologic ascorbate were escalated utilizing Storer's phase I clinical trial design BD (Storer, 1989). Cohorts were defined as 15 g, 25 g, 50 g, 62.5 g, 75 g, 87.5 g, 100 g, and 125 g. Pharmacologic ascorbate was combined with sterile water for a targeted osmolarity of 500-900 mOsm $L^{-1}$. Ascorbate infusions were three times weekly, with maximum infusion rate of 500 mL $hr^{-1}$. Radiation (61.2 Gy in 34 fractions) and temozolomide (75 mg $m^{-2}$ daily for a maximum of 49 days) similar to the treatment paradigm put forth by Stupp et al. (Stupp et al., 2005) (Figure 7A). After completing radiation, ascorbate infusions were reduced to twice weekly; dose remained unchanged from the radiation phase.

Adjuvant phase was defined as the time period from cycle 1 day 1 through cycle 6 day 28. During this phase, subjects underwent intrapatient escalation utilizing Simon's Accelerated Titration Design (Simon et al., 1997). Prescribed doses utilized the same cohorts as the radiation phase. Subjects were dose-escalated after 2 infusions until a plasma level of 20 mM was achieved. Ascorbate infusions were performed twice weekly. Temozolomide was prescribed consistent with the Stupp regimen: 150 mg $m^{-2}$ for days 1 through 5 of a 28 day cycle. A one-time dose escalation was allowed to 200 mg $m^{-2}$ if cycle 1 was tolerated (Figure 7A). Subjects were evaluated for disease progression every 2 cycles utilizing the MacDonald criteria (Macdonald et al., 1990).

On a given day, during the radiation phase, GBM subjects received ascorbate infusions of 30 – 180 min in duration (depending on the total dose) followed by radiation therapy. The dose escalation aspect of the study and the maximum infusion rate of ascorbate at 50 g $hr^{-1}$ required this range of infusion times. The protocol did not specify when the radiation was to be administered relative to the infusion time, so for higher ascorbate doses, requiring longer infusion times (> 50 g), the subject received radiation therapy during the last hour of ascorbate infusion or immediately following infusion. Temozolomide chemotherapy was administered orally in the evening by the patient at home and the time between ascorbate infusion and temozolomide administration was not defined. This timing of ascorbate and temozolomide was continued throughout the adjuvant phase.

MGMT status was determined by a PCR-based analysis at ARUP National Reference Laboratory (Salt Lake City, UT). IDH subject status was determined immunohistochemically by the University of Iowa Hospitals and Clinics Clinical Histopathology Laboratory.

Dose limiting toxicities (DLTs) for the study included grade 4 infection, grade 3 nausea or vomiting despite maximum supportive care, grade 4 neutropenia or thrombocytopenia, and serious adverse events (SAE) with causality to the investigational agent. In addition to DLT, criteria for removal included progressive disease, patient's refusal to continue treatment, and extraordinary medical circumstances (e.g., the constraints of the protocol are considered detrimental to patient health).

All subjects agreed to, and participate in, lifelong follow-up for this study. Subject numbers are for convenience and are not representative of case ID numbers. Subjects 12 and 13 (Table S2) are included in the toxicity analysis (Tables S3 and S4), but were not included in the progression free survival and overall survival analysis (Figures 7A, 7C, and 7D) because they received limited protocol-dictated therapy due to unrelated co-morbidities. Due to the small number of subjects in the longevity analysis we reported the average progression free survival (PFS) and overall survival (OS).

### Phase II Clinical Trial of Pharmacological Ascorbate in Combination with Chemotherapy as a First Line Treatment in Advanced Stage NSCLC

This phase II clinical trial is being conducted at the University of Hospitals and Clinics to evaluate the efficacy of combining carboplatin and paclitaxel with pharmacological ascorbate in advanced stage (stage IIIB and IV) NSCLC patients. Approval was sought, and obtained, from the University of Iowa Institutional Review Board (Biomedical IRB-01; IRB 201412760). This phase II clinical trial was registered with clinicaltrials.gov (NCT 02420314) prior to enrollment of the first subject. Newly diagnosed advanced stage NSCLC patients were invited to participate. Post-consent screening procedures included evaluating for glucose-6-phosphatase dehydrogenase deficiency as well as osmolarity tolerance by challenging the consented subjects with a 15 g ascorbate infusion.

The study included treating patients with 4 cycles of carboplatin AUC 6 and paclitaxel 200 mg $m^{-2}$ every 21 days as first line chemotherapy combined with pharmacological ascorbate. Ascorbate was administered intravenously twice per week at a fixed dose of 75 g per infusion for 6 treatments per each 21 days cycle of chemotherapy. Pharmacologic ascorbate was combined with sterile water for a targeted osmolarity of 500-900 mOsm/L. Blood ascorbate levels and measures of reactive oxygen species were collected each cycle from subjects immediately prior to and after completing ascorbate infusions. On a given therapy day, chemotherapy infusions (paclitaxel followed by carboplatin) were initiated ~1 hr following the completion of the ascorbate infusions.

So far, no grade 3/4 toxicities attributed to ascorbate have occurred. The regimen is well tolerated and no patients have withdrawn consent due to toxicities. We have not seen any unexpected or unusual increase in Grade 3/4 toxicities as compared to previously published literature, although it remains too early for a direct comparison. Responses to therapy were determined per RECIST 1.1

criteria (Eisenhauer et al., 2009). Currently, a total of fourteen subjects are currently evaluable for response. Four of fourteen subjects have completed the trial with imaging-confirmed partial responses to therapy. Nine additional subjects demonstrated stable disease. Finally, one subject has progressed with the appearance of new lesions, although the target lesions are stable. All subjects agreed to, and participate in, lifelong follow-up for this study.

## QUANTIFICATION AND STATISTICAL ANALYSIS

For all analyses, significance was determined at $p < 0.05$. *, **, or *** represent significance between exposure conditions. All analyses, unless specified elsewhere, were performed in GraphPad Prism® (GraphPad Software, Inc.). Ascorbate toxicity curves (Figures 1A and 1B) were generated using IGOR Pro version 6.36 (WaveMetrics, Inc.).

Where appropriate, figure legends define n and the definition of center and dispersion and precision measures. For analyses limited to two groups, Student's *t*-test was utilized. To study differences between three or more groups, one-way ANOVA analysis with Tukey's post hoc test was used. For all survival curves, the log-rank Mantel-Cox test was used. For NSCLC LIP curves (Figure 6A) and GBM/NHA toxicity curves (Figure S1D) non-linear regression curves were compared by the extra sum-of-squares F test. For GBM and NSCLC-Ft LIP curves (Figures 6B and 6K) deviation from non-zero slope was determined from linear regression analyses. Box and whisker blot of patient plasma ascorbate concentrations (Figure 7B) are determined by the Tukey method. The line and box represent the median value ± $25^{th}$ and $75^{th}$ percentiles or the interquartile range (IQR). Whiskers represent 1.5 times IQR. Any data points outside 1.5 times IQR are represented by individual dots.

Data are expressed as mean ± 1 S.E.M., unless otherwise specified. For each experiment, unless otherwise noted, n represents the number of individual biological replicates. For each biological replicate, $n \geq 3$ technical replicates for all in vitro and ex vivo studies.

For GBM subject survival analyses, Subjects 12 and 13 (Table S2) are included in the toxicity analysis (Tables S3 and S4), but were not included in the progression free survival and overall survival analysis (Figures 7A, 7C, 7D) because they received limited protocol-dictated therapy due to unrelated co-morbidities.

## ADDITIONAL RESOURCES

A Phase I Clinical Trial of High-Dose Ascorbate in Glioblastoma Multiforme (NCT01752491): https://clinicaltrials.gov/ct2/show/NCT01752491

Pharmacological Ascorbate for Lung Cancer (NCT02420314): https://clinicaltrials.gov/ct2/show/NCT02420314